

N70-30153
NASA-CR-110406

REPORT 69-77



AEROSPACE ENGINEERING DEPARTMENT

TEXAS A&M UNIVERSITY

NONLINEAR DYNAMIC ANALYSIS OF SHELLS OF REVOLUTION
BY MATRIX DISPLACEMENT METHOD

by

J. A. Stricklin, J. E. Martinez, J. R. Tillerson,
J. H. Hong, and W. E. Haisler

FEBRUARY 1970

CASE FILE
COPY

TEXAS ENGINEERING EXPERIMENT STATION

NONLINEAR DYNAMIC ANALYSIS OF SHELLS OF REVOLUTION
BY MATRIX DISPLACEMENT METHOD

J. A. Stricklin,* J. E. Martinez,** J. R. Tillerson,***
J. H. Hong,*** and W. E. Haisler***

Texas A&M University
College Station, Texas

November 24, 1969

- * Professor, Aerospace Engineering Department
- ** Assistant Professor, Civil Engineering Department
- *** Research Assistant, Aerospace Engineering Department

ACKNOWLEDGEMENT

This research was supported under Sandia Contract 82-2930, Sandia Corporation, Albuquerque, New Mexico and NASA Grant NGL-44-001-044, Manned Spacecraft Center, Houston, Texas

Appreciation is expressed to Dr. Walter Von Riesemann of Sandia and Dr. Fred Stebbins of Manned Spacecraft Center, who served as technical monitors for the research. Appreciation is also expressed to Dr. Sam Key and Dr. Ray Krieg of Sandia for their helpful suggestions during the course of this research.

ABSTRACT

A formulation and computer program is developed for the geometrically nonlinear dynamic analysis of shells of revolution under symmetric and asymmetric loads. The nonlinear strain energy expression is evaluated using linear functions for all displacements. Five different procedures are examined for solving the equations of equilibrium with Houbolt's method proving to be the most suitable. Solutions are presented for the symmetrical and asymmetrical buckling of shallow caps under step pressure loadings and a wide variety of other problems including some highly nonlinear ones.

TABLE OF CONTENTS

	page
	ii
ACKNOWLEDGEMENT	ii
ABSTRACT	iii
NOMENCLATURE	vi
INTRODUCTION	1
FORMULATION OF PROBLEM	5
General Development	5
Mass Matrix	8
Nonlinear Terms	11
Thermal Terms	17
Stress Resultants	23
METHODS OF SOLUTION	27
Houbolt's Method	31
Chan, Cox and Benfield Method	33
Runge-Kutta Method	35
Approximation of Loads Matrix	36
Numerical Results	37
APPLICATIONS	47
COMPUTER PROGRAM	53
CONCLUSIONS	57
REFERENCES	58
FIGURES	61
APPENDIX A. Mass Matrix	
APPENDIX B. Linear Thermal Loads	

	page	
LIST OF FIGURES		
1	Meridional Stress Along Arc Length	61
2	Meridional Stress Along Arc Length	62
3	Meridional Stress Along Arc Length	63
4	Meridional Stress Along Arc Length	64
5	Deflection Along Axis of Symmetry	65
6	Generalized Coordinates of Shell Element	66
7	Displacement Response Calculated by Two Numerical Methods	67
8	Circumferential Stress Resultant For Shell Under Step Pressure Loading	68
9	Meridional Shear Resultant For Shell Under Step Pressure Loading	69
10	Static Response of Shallow Spherical Cap	70
11	Effect of Numerical Accuracy Upon Shell Response at Apex	71
12	Effect of Load Extrapolation Procedure Upon Apex Axial Displacement	72
13	Solution Convergence with Finite Element Idealization	73
14	Effect of Time Increment Upon Apex Axial Displacement	74
15	Shallow Spherical Cap Under Axisymmetric Dynamic Loading	75
16	Nondimensional Fourier Coefficient of Normal Displacement Versus Time For Cylinder Under Asymmetrical Loading	76
17	Critical Pressure Ratio as a Function of the Shallow Shell Parameter	77
18	Response of 2nd Harmonic for Various Pressure Ratios	78
19	Peak Response of Harmonic 0 and 2 for Different Pressure Ratios	79
20	Displacement Response for a Cylinder Subjected to Suddenly Applied Axial Load	80
21	Axial Displacement Along Cylinder at 50.0 Microseconds	81
22	Axial Stress Distribution Along Cylinder at 50.0 Microseconds	82
23	Vertical Deflection for Spherical Cap Under Localized Loading	83
24	Meridional Stress Resultant for Spherical Cap Under Localized Loading	84
25	Circumferential Stress Resultant for Spherical Cap Under Localized Loading	85
26	Circumferential Moment for Spherical Cap Under Localized Loading	86
27	Meridional Moment for Spherical Cap Under Localized Loading	87

NOMENCLATURE

[]	=	row matrix
[]	=	square matrix
{ }	=	column matrix
[A]	=	transformation matrix
[]'	=	matrix transpose
C_1	=	$E_s t / (1 - \nu_{s\theta} \nu_{\theta s})$
C_2	=	$E_\theta t / (1 - \nu_{s\theta} \nu_{\theta s})$
[D]	=	elasticity matrix
D_1	=	$E_s t^3 / [12(1 - \nu_{s\theta} \nu_{\theta s})]$
D_2	=	$E_\theta t^3 / [12(1 - \nu_{s\theta} \nu_{\theta s})]$
E	=	Young's modulus
\hat{e}	=	linear strains and rotations
F	=	pressure loading on shell
G	=	shear modulus
G_1	=	Gt
G_2	=	Gt^3
K	=	changes in curvature
[K]	=	stiffness matrix
L	=	meridional length of shell element
[M]	=	mass matrix
M	=	moment resultants
N	=	stress resultants
Q	=	shear resultants

$\{Q\}$	=	generalized forces
$\{q\}$	=	nodal displacements
$\{\dot{q}\}$	=	nodal velocities
$\{\ddot{q}\}$	=	nodal accelerations
r	=	cylindrical coordinate
s	=	meridional distance along shell element
t	=	shell thickness and time
T	=	kinetic energy and temperature
T'	=	temperature gradient
U	=	internal energy
u, v, w	=	displacements in meridional, circumferential and normal directions, respectively
$\dot{u}, \dot{v}, \dot{w}$	=	velocities in meridional, circumferential, and normal directions, respectively
α	=	generalized displacement coefficients
$\dot{\alpha}$	=	generalized velocity coefficients
α_s	=	coefficient of thermal expansion in meridional direction
α_θ	=	coefficient of thermal expansion in circumferential direction
β	=	parameter of generalized acceleration used in numerical method given in Ref. 20
Δt	=	time increment
ϵ	=	midsurface strains
θ	=	circumferential angle
ν	=	Poisson's ratio
ρ	=	mass density
ϕ	=	slope of undeformed shell
ϕ'	=	$\frac{d\phi}{ds}$

Subscripts and Superscripts

e	=	element
L	=	linear and at $s = L$
NL	=	nonlinear
m	=	middle of element and degree of freedom of element
n	=	harmonic number
o	=	initial value
s	=	meridional direction
t	=	thermal effect
θ	=	circumferential direction

INTRODUCTION

The geometrically nonlinear static analysis of structures has made considerable progress since the original finite element paper by Turner, Dill, Martin, and Melosh.¹ In Ref. 1, it was proposed that the nonlinear problem be analyzed as a sequence of linear problems using a geometric stiffness matrix. This approach has been used by many investigators in more recent years and has been refined to a very high degree. In fact, it is safe to say that the geometric stiffness method approach is the most widely used method for the geometrically nonlinear analysis of structures by the matrix displacement method with the Newton-Raphson method of solution being a distant second. Rather exhaustive survey articles on the nonlinear analysis of structures by matrix methods have been presented by Martin² and Oden.³

For a shell of revolution under asymmetrical loading, the incremental stiffness method is difficult to apply due to the coupling which the nonlinear terms introduce among the various Fourier harmonics. This gives rise to a large number of equations which must be solved after new coefficients are generated at each load increment. For example, twenty harmonics and fifty elements would give rise to 4080 equations of equilibrium.

The difficulty of repeated solutions of a large number of equations has been circumvented by Stricklin, Haisler, MacDougall, and Stebbins⁴ who place the nonlinear terms on the right-hand side of the equations of equilibrium and treat them as additional loads. The method of solution is by iteration and has been found to yield accurate results for a large majority of practical problems. For highly nonlinear problems, the

equations as formulated in Ref. 4 are currently being solved by the Newton-Raphson procedure with the coupling between harmonics being ignored. The present paper presents an extension of the work presented in Ref. 4 to the nonlinear dynamic analysis of shells of revolution under both symmetric and asymmetric loadings. It will be demonstrated that the approach presented herein is valid for highly nonlinear problems. It is assumed in the present work that the material is elastic and nonlinearities are due to moderate rotations.

Computer programs for the large deflection elastic-plastic analysis of beams, rings, and plates have been developed by Witmer, Balmer, Leech, and Pian⁵ and Krieg and Duffey.⁶ In Refs. 5 and 6, the governing equations of motion are written in finite difference form in both space and time. The solution is straight-forward in that the equations are solved sequentially with no coupling existing between equations. Correlation studies have been conducted by Duffey and Key,⁷ Krieg, Duffey, and Key,⁸ and Balmer and Witmer.⁹ The correlation studies have demonstrated that the computer programs as developed in Refs. 5 and 6 may be used to compute adequately the large deflection dynamic response of highly nonlinear elastic-plastic simple structures.

Leech, Witmer, and Pian¹⁰ and Wrenn, Sobel and Silsby¹¹ have presented formulations and computer programs for the nonlinear analysis of general thin shells. The equations governing the response of a shell under arbitrary impulsive loading are developed in tensor form and represented by finite differences in space and time. Solutions are presented for a cylindrical panel¹⁰ and a cylinder.¹¹ In addition to finite differences in

time, the Adams-Moulton and fourth order Runge-Kutta methods were used in Ref. 11. An interesting conclusion drawn in Ref. 11 is that the size of the time increment needed for numerical stability in the finite difference method of solution is smaller than the time increment needed to prevent excessive truncation error.

Stability studies on the different methods used to approximate the second derivatives in time have recently been conducted by Leech, Hsu, and Mack,¹² Johnson,¹³ Krieg,¹⁴ and Nickell.¹⁵ However, with the exception of Ref. 14, the studies have been limited to the linear equations of motion and are not applicable to the nonlinear analysis. In particular, the unconditional stability exhibited by Houbolt's¹³ and Neumark's¹⁵ ($\gamma = \frac{1}{2}$, $\beta = \frac{1}{4}$) methods for the linear case does not exist in the nonlinear formulation presented in this report.

It is apparent from the cited references that considerable progress has been made in analyzing the elastic-plastic nonlinear dynamic behavior of shells using finite differences in the spatial coordinates. However, little progress has been made in the analysis of the nonlinear dynamic behavior of shells through the finite element approach. Further, there does not seem to exist any computer program which is capable of analyzing the nonlinear asymmetrical dynamic behavior of shells of revolution in a reasonable period of computer time. The purpose of the present paper is to present such a program and demonstrate through examples its range of applicability.

The research presented here uses the curved element of Stricklin, Navaratna, and Pian¹⁶ and the displacement function of Grafton and Strome.¹⁷

The nonlinear shell theory of Novozhilov¹⁸ is assumed to be applicable with the further assumption of small strains and moderate rotations being made. Reference 4 presents a more complete review of the pertinent literature and a detailed description of the theoretical formulation. However, missing from Ref. 4 are the discussions of the works on the linear dynamic analysis of shells of revolution by Klein and Sylvester¹⁹ and Popov and Chow.* Klein and Sylvester use the method of Chan, Cox and Benfield²⁰ to solve the equations of equilibrium whereas Popov and Chow use the modal analysis. The results obtained by both methods which are presented in Ref. 19 are in good agreement for a spherical cap under a step pressure loading. This same problem is analyzed herein and the results are presented in a later section.

In the earlier stages of the research presented herein, the method of Ref. 20 was used for solutions. In fact, a technical note²¹ has been published on the axisymmetric dynamic buckling of shallow caps under step pressure loading in which the method of Ref. 20 is used to solve the equations of equilibrium. However, more recent studies have shown that Houbolt's method²² is more stable and thereby more efficient than the method of Ref. 20 for solving highly nonlinear problems. Consequently, most of the results presented in this report are based on Houbolt's method of solution.

*Presented as Addendum in Reference 19.

FORMULATION OF PROBLEM

General Development

The purpose of this section is to present a concise formulation of the problem, omitting most of the detailed discussion, but enabling the reader to obtain a basic knowledge of the overall problem. Detailed derivations are presented in later sections.

The nonlinear dynamic and thermal analysis of shells of revolution may be simplified by employing the static analysis and extending it to include dynamic and thermal effects.

The equations of equilibrium for the static case are of the form

$$[K^n]\{q^n\} = \{Q^n\} - \left\{ \frac{\partial U_{NL}}{\partial q^n} \right\} \quad (1)$$

and inclusion of the inertia and thermal terms yields the equations of motion as

$$[M^n]\{\ddot{q}^n\} + [K^n]\{q^n\} = \{Q^n\} + \{Q_t^n\} - \left\{ \frac{\partial U_{NL}}{\partial q^n} \right\} + \left\{ \frac{\partial U_{NL}^t}{\partial q^n} \right\} \quad (2)$$

where

$[M^n]$ = symmetric mass matrix for harmonic n

$\{\ddot{q}^n\}$ = column matrix of generalized accelerations for harmonic n

$[K^n]$ = symmetric stiffness matrix for harmonic n

$\{q^n\}$ = column matrix of generalized displacements for harmonic n

$\{Q^n\}$ = column matrix of generalized forces for harmonic n

$\{Q_t^n\}$ = column matrix of linear thermal pseudo loads for harmonic n

$\{\frac{\partial U_{NL}}{\partial q^n}\}$ = column matrix of generalized pseudo forces due to nonlinearities

$\{\frac{\partial U_{NL}^t}{\partial q^n}\}$ = column matrix of thermal pseudo loads due to nonlinear terms in expressions for midsurface strains

The second and fourth terms of the right-hand side of Eq. 2 result from considering the strain energy expression as

$$U = U_L - U_L^t + U_{NL} - U_{NL}^t \quad (3)$$

where

U_L = strain energy using linear theory

U_L^t = strain energy which accounts for thermal effects using linear theory

U_{NL} = strain energy due to addition of nonlinear terms in midsurface strains

U_{NL}^t = strain energy which accounts for thermal effects resulting from nonlinear terms in midsurface strains

The element mass matrix has been derived using energy principles and includes the effects of rotary inertia. The element stiffness matrix is obtained from the expression for U_L . Both matrices are computed in the first part of the computer code called DYNASOR I (DYnamic Nonlinear Analysis of Shells Of Revolution) which generates mass and stiffness matrices and geometric properties and writes them on tape for input to the second part of the code, DYNASOR II.

The term $\{Q^n\}$ represents generalized forces arising from mechanical loads and is evaluated by considering the work potential due to external forces to be the same as in linear theory and following the procedure outlined in Ref. 4. The term $\{Q_t^n\}$ is evaluated exactly from $\frac{\partial U_L^t}{\partial q^n}$.

A detailed discussion of the computation of the thermal loads is presented in a later section.

The term $\{\frac{\partial U_{NL}}{\partial q_n}\}$ which represents the generalized pseudo forces due to nonlinearities is obtained by retaining strain energy terms containing the rotations raised to the fourth power. The evaluation is performed by using linear functions for all displacements and strip integration over the length of the element, whereas integrals in the circumferential direction are evaluated exactly. This and the fact that the meridional and normal displacements are represented by only a Fourier cosine series and the tangential displacements by a sine series in the circumferential angle θ , make the procedure different from the one employed in the static case which is described in Ref. 4. The application of boundary conditions to the zero harmonic has also been modified for the case of a closed shell. In this instance the radial displacement and angular rotation at the apex in the zero harmonic are specified as being zero in the initial information to DYNASOR II. This is a known boundary condition and is specified to assure better numerical stability for the highly nonlinear problems. This new formulation permits accurate results and circumvents the problem of having to resort to secondary storage on the computer. The code for the IBM 360/65 presently allows the solution of a problem requiring five Fourier harmonics which may be selected from a set of twenty and it may be extended to include ten without encountering storage difficulties on computers.

such as the CDC 6600 where double precision is not needed. The zero harmonic must be included in the set.

Several methods for numerically integrating the equations of motion were investigated and Houbolt's method was found to be the best. This method permits use of a reasonable time increment without encountering numerical instability. If a particular time increment is found to be numerically unstable, a restart option of the computer code allows the program to be restarted from a certain time with a reduced interval of time.

Considerable time has been devoted to optimizing the computer operations in the various subroutines and the net result is a computer code that yields accurate results to complex problems in short periods of time. Few problems require more than 30 minutes of time on the IBM 360/65 computer.

Mass Matrix

The element mass matrix, which includes the effects of rotary inertia, may be obtained by considering the expression for the kinetic energy

$$T = \frac{1}{2} \int_V (\dot{u}^2 + \dot{v}^2 + \dot{w}^2) dm \quad (4)$$

where the velocities, \dot{u} , \dot{v} , and \dot{w} , are given by

$$\begin{aligned}\dot{w} &= \dot{w}_0 \\ \dot{u} &= \dot{u}_0 + z \dot{\hat{e}}_{13} \\ \dot{v} &= \dot{v}_0 + z \dot{\hat{e}}_{23}\end{aligned}\tag{5}$$

and

$$\begin{aligned}\dot{\hat{e}}_{13} &= \frac{d}{dt} \left(\frac{\partial w_0}{\partial s} + \phi' u_0 \right) \\ \dot{\hat{e}}_{23} &= \frac{d}{dt} \left[\frac{1}{r} \left(\frac{\partial w_0}{\partial \theta} - v_0 \cos \phi \right) \right] \\ \dot{w}_0 &= \sum_{i=0} (\dot{\alpha}_1^i + \dot{\alpha}_2^i s + \dot{\alpha}_3^i s^2 + \dot{\alpha}_4^i s^3) \cos i\theta \\ \dot{u}_0 &= \sum_{i=0} (\dot{\alpha}_5^i + \dot{\alpha}_6^i s) \cos i\theta \\ \dot{v}_0 &= \sum_{i=0} (\dot{\alpha}_7^i + \dot{\alpha}_8^i s) \sin i\theta\end{aligned}\tag{6}$$

and

dm = differential mass element

i = integer corresponding to terms being used in Fourier expansion - must include $i = 0$.

The sum is over the total number of harmonics used.

Substituting Eqs. 5 and 6 into Eq. 4, the kinetic energy may be expressed as a quadratic form in the generalized velocity coefficients, $\dot{\alpha}_n$, as

$$T = \frac{1}{2} [\dot{\alpha}] [\bar{M}] \{\dot{\alpha}\} \quad (7)$$

The $\{\dot{\alpha}\}$ matrix is related to the velocities of the generalized structural coordinates, $\{\dot{q}\}$, by the transformation

$$\{\dot{\alpha}\} = [A] \{\dot{q}\} \quad (8)$$

The matrix $[A]$ is given in Ref. 4 and the elements of $[\bar{M}]$ are listed in the Appendix A.

When rotary inertia is included, the element mass matrix becomes a function of the harmonic number and a different element mass matrix must be calculated for each Fourier harmonic. This computation is carried out by first expressing the kinetic energy in terms of the generalized velocity coefficients, $\dot{\alpha}_n$, and then employing the same congruent transformation used for element stiffness matrices. In this manner, the element mass matrix may be expressed as

$$[M^e] = [A]' [\bar{M}] [A] \quad (9)$$

This calculation, along with the computation of element stiffness matrices and geometric properties, is performed in the first part of the computer code, DYNASOR I.

Nonlinear Terms

Two major changes in the treatment of the forces due to nonlinearities have been made over that presented in Ref. 4. These are:

1. The fourth order terms in the strain energy expression are retained. It has been found during the course of this investigation that the retention of the fourth order terms is absolutely essential for all problems where the nonlinear terms are substantial. For example, as reported in Ref. 21, for a shallow shell parameter of 7.5, the ratio of the dynamic buckling load to the classical static buckling load changes from .38 to .50 when the fourth order terms are included.

The significance of the fourth order terms in the static solution of cap-torus-cylinder configurations under symmetric and asymmetrical loads is illustrated in Figs. 1-5. These results are for the same problems presented in Ref. 4 and, after including the fourth order terms, agree exactly with the results presented by Bushnell.²³ All the copies of the computer program for the nonlinear static analysis released by Texas A&M University include the fourth order terms.

2. The generalized forces due to nonlinearities are evaluated using linear displacement functions in all variables and strip integration over the length of the element. The integrals around the circumference are evaluated in closed form for the particular harmonics chosen. This simplification over that presented in Ref. 4 permits the forces due to nonlinearities to be evaluated without the use of auxiliary computer storage. The purpose of the remainder of this section is to discuss the nature of the approximation and present the details of the derivation.

The strain energy of an element due to nonlinearities in the strain-displacement relation, including the fourth order terms, is given by

$$\begin{aligned}
 U_{NL} = & \frac{1}{2} \int \int [C_1 \hat{e}_s \hat{e}_{13}^2 + C_2 \hat{e}_\theta \hat{e}_{23}^2 + v_{s\theta} C_1 (\hat{e}_s \hat{e}_{23}^2 + \hat{e}_\theta \hat{e}_{13}^2) \\
 & + 2G_1 \hat{e}_{s\theta} \hat{e}_{13} \hat{e}_{23} + \frac{1}{4} C_1 \hat{e}_{13}^4 + \frac{1}{4} C_2 \hat{e}_{23}^4] \\
 & + (\frac{1}{2} v_{s\theta} C_1 + G_1) \hat{e}_{13}^2 \hat{e}_{23}^2 r ds d\theta
 \end{aligned} \tag{10}$$

where \hat{e}_s , \hat{e}_θ , and $\hat{e}_{s\theta}$ are the expressions for the meridional, circumferential, and shear strain based on linear theory.

\hat{e}_{13} and \hat{e}_{23} are rotations about the circumferential and meridional coordinates, respectively.

C_1 , C_2 , G_1 , and $v_{s\theta}$ are material constants.

s and θ are meridional and circumferential coordinates as shown in Fig. 6

The generalized forces due to the nonlinearities are given by

$\frac{\partial U_{NL}}{\partial q_m^n}$ where m is the degree of freedom for the element (Fig. 6) and n is the harmonic number. Applying the operation to the strain energy yields

$$\begin{aligned}
 \frac{\partial U_{NL}}{\partial q_m^n} = & \frac{1}{2} \int \int \{ (C_1 \hat{e}_{13}^2 + v_{s\theta} C_1 \hat{e}_{23}^2) \frac{\partial \hat{e}_s}{\partial q_m^n} \\
 & + (C_2 \hat{e}_{23}^2 + v_{s\theta} C_1 \hat{e}_{13}^2) \frac{\partial \hat{e}_\theta}{\partial q_m^n} + 2G_1 \hat{e}_{13} \hat{e}_{23} \frac{\partial \hat{e}_{s\theta}}{\partial q_m^n} \\
 & + (2C_1 \hat{e}_s \hat{e}_{13} + 2v_{s\theta} C_1 \hat{e}_\theta \hat{e}_{13} + 2G_1 \hat{e}_{s\theta} \hat{e}_{23}) \frac{\partial \hat{e}_{13}}{\partial q_m^n}
 \end{aligned} \tag{11}$$

$$\begin{aligned}
& + (2C_2 \hat{e}_\theta \hat{e}_{23} + 2v_{s\theta} C_1 \hat{e}_s \hat{e}_{23} + 2G_1 \hat{e}_{s\theta} \hat{e}_{13}) \frac{\partial \hat{e}_{23}}{\partial q_m^n} \} r ds d\theta \\
& + \frac{1}{2} \int \{ [C_1 \hat{e}_{13}^3 + (v_{s\theta} C_1 + 2G_1) \hat{e}_{13} \hat{e}_{23}^2] \frac{\partial \hat{e}_{13}}{\partial q_m^n} \\
& + [C_2 \hat{e}_{23}^3 + (v_{s\theta} C_1 + 2G_1) \hat{e}_{13}^2 \hat{e}_{23}] \frac{\partial \hat{e}_{23}}{\partial q_m^n} \} r d\theta ds
\end{aligned} \tag{11}$$

In this research, only the cosine terms for u and w and the sine terms for v are retained in the expansion. Thus, substituting Eqs. 19 of Ref. 4, using strip integration over the meridional length, s, and evaluating the trigonometric integrals around the circumference, the forces on the element due to nonlinearities become

$$\begin{aligned}
\frac{\partial U_{NL}}{\partial q_m^n} &= \frac{r_m L}{2} \sum_{i=0} \sum_{j=0} \{ (C_1^{ijn} e_{13}^i e_{13}^j + v_{s\theta} \bar{C}_1^{ijn} e_{23}^i e_{23}^j) \frac{\partial e_s^n}{\partial q_m^n} \\
& + (\bar{C}_2^{ijn} e_{23}^i e_{23}^j + v_{s\theta} \bar{C}_1^{ijn} e_{13}^i e_{13}^j) \frac{\partial e_\theta^n}{\partial q_m^n} + 2 \bar{G}_1^{ijn} e_{13}^i e_{23}^j \frac{\partial e_{s\theta}^n}{\partial q_m^n} \\
& + (2 \bar{C}_1^{ijn} e_s^i e_{13}^j + 2v_{s\theta} \bar{C}_1^{ijn} e_\theta^i e_{13}^j + 2 \bar{G}_1^{ijn} e_{s\theta}^i e_{23}^j) \frac{\partial e_{23}^n}{\partial q_m^n} \\
& + (2 \bar{C}_2^{ijn} e_\theta^i e_{23}^j + 2v_{s\theta} \bar{C}_1^{ijn} e_s^i e_{23}^j + 2 \bar{G}_1^{ijn} e_{s\theta}^i e_{13}^j) \frac{\partial e_{23}^n}{\partial q_m^n} \}
\end{aligned} \tag{12}$$

$$\begin{aligned}
 & + \frac{r_m L}{2} \sum_{i=0} \sum_{j=0} \sum_{k=0} \{ \bar{C}_1^{ijkn} e_{13}^i e_{13}^j e_{13}^k \\
 & + (v_{s\theta} \bar{C}_1^{ijkn} + 2 \bar{G}_1^{ijkn}) e_{13}^i e_{23}^j e_{23}^k \} \frac{\partial e_{13}^n}{\partial q_m^n} \\
 & + [\bar{C}_2^{ijkn} e_{23}^i e_{23}^j e_{23}^k + (v_{s\theta} \bar{C}_1^{ijkn} + 2 \bar{G}_1^{ijkn}) e_{13}^i e_{13}^j e_{23}^k] \frac{\partial e_{23}^n}{\partial q_m^n} \}
 \end{aligned} \quad (12)$$

where r_m = value of r at middle of element

L = length of element

e^i = coefficient of $\sin i\theta$ or $\cos i\theta$ in the expressions for the strains and rotations for harmonic i at the middle of the element

The superscripts over the material constants, C_1 , C_2 , G_1 indicate that the material constant is multiplied by the integral of the trigonometric functions. For example,

$$\bar{C}_1^{ijkn} = C_1 \int_0^{2\pi} \cos i\theta \cos j\theta \cos k\theta \cos n\theta d\theta \quad (13)$$

A bar over i , j , k , or n indicates that $\cos\theta$ is replaced by $\sin\theta$ in the integral. The strains and rotations are evaluated at the center of the element.

The evaluation of the strains at the center of the element and consequently, their partial derivatives with respect to the generalized coordinates presented a difficulty. For example, the rotation e_{13} may be approximated in alternate forms as

$$e_{13}^i = \frac{q_4^i + q_8^i}{2} \quad (14)$$

or $e_{13}^i = \frac{q_7^i \cos\phi_L - q_5^i \sin\phi_L - q_3^i \cos\phi_o + q_1^i \sin\phi_o}{L}$

$$+ \frac{(q_7^i \sin\phi_L + q_5^i \cos\phi_L + q_3^i \sin\phi_o + q_1^i \cos\phi_o)}{2} \phi_m'$$
(15)

where subscripts o, L, and m refer to the term evaluated at $s = 0$, $s = L$, and $s = \frac{L}{2}$ respectively. The superscript refers to the i th harmonic.

While little difference will be observed in the evaluation of e_{13} between the two alternate forms, the partial derivatives are completely different. Both methods were used at the beginning of this research and a considerable difference was observed in the results.

To resolve the difficulty of which form to use, the following was considered. The strain energy expression U_{NL} depends only on first derivatives. Consequently in the evaluation of U_{NL} , it is necessary to satisfy only continuity of displacements between elements and not continuity of slopes.²⁴ This allows the use of linear displacement functions in s for w as well as u and v . Using linear displacement functions for all the variables, it is the second form, given by Eq. 15, for e_{13} which is obtained and used in this research.

The following expressions are used for the strains and rotations

$$e_s^i = \frac{q_7^i \sin\phi_L + q_5^i \cos\phi_L - q_3^i \sin\phi_o - q_1^i \cos\phi_o}{L}$$

$$- \frac{(q_7^i \cos\phi_L - q_5^i \sin\phi_L + q_3^i \cos\phi_o - q_1^i \sin\phi_o)}{2} \phi_m'$$

$$\begin{aligned}
e_{\theta}^i &= \frac{1}{r_m} [i \frac{q_2^i + q_6^i}{2} + \\
&\quad (\frac{q_7^i \sin\phi_L + q_5^i \cos\phi_L + q_3^i \sin\phi_o + q_1^i \cos\phi_o}{2}) \sin\phi_m \\
&\quad + (\frac{q_7^i \cos\phi_L - q_5^i \sin\phi_L + q_3^i \cos\phi_o - q_1^i \sin\phi_o}{2}) \cos\phi_m] \\
e_{s\theta}^i &= \frac{1}{r_m} [-i (\frac{q_7^i \sin\phi_L + q_5^i \cos\phi_L + q_3^i \sin\phi_o + q_1^i \cos\phi_o}{2}) \\
&\quad - \frac{q_2^i + q_6^i}{2r_m} \sin\phi_m + \frac{q_6^i - q_2^i}{L}]
\end{aligned} \tag{16}$$

$$e_{13}^i = \text{Eq. 15}$$

$$\begin{aligned}
e_{23}^i &= \frac{1}{r_m} [-i (\frac{q_7^i \cos\phi_L - q_5^i \sin\phi_L + q_3^i \cos\phi_o - q_1^i \sin\phi_o}{2}) \\
&\quad - \frac{q_2^i + q_6^i}{2} \cos\phi_m]
\end{aligned}$$

Equations 16 were obtained from Eqs. 8 of Ref. 4 by using linear displacement functions, applying a coordinate rotation to u and w , and evaluating the results at the middle of the element.

The calculation procedure within the computer code consists of evaluating the partial derivatives of the strains and rotations with respect to each and every q^i and then evaluating the strains and rotations as the sum of their partial derivatives with respect to the generalized

coordinates times the generalized coordinates. These partial derivatives, strains, and rotations are used in the evaluation of Eq. 12, the stress resultant routine, and in the evaluation of the nonlinear thermal terms.

In Eq. 12, the fourth order terms yield a triple sum over the number of harmonics. Fortunately, most of the integrals around the circumference of the shell are zero and may be omitted in the calculation.

In summary, due to the exact evaluation of the integrals in the circumferential direction it is reasonable to expect rapid convergence as the number of harmonics is increased. It will be demonstrated through a numerical example in a later section that the use of strip integration over the length of the element produces convergence quite rapidly as the number of elements is increased.

Thermal Terms

This section describes the derivations of the linear and nonlinear thermal loads. The thermal loads are evaluated for each element and then combined at the nodes for the entire structure.

Temperature Distribution

The temperature distributions at the midsurface, T , and the temperature gradients in the normal direction, T' , for an element are expanded in a Fourier series in a manner similar to that used for the displacement functions. The expressions may be written as

$$T = \sum_{i=0}^{\infty} T^i \cos i\theta \quad (17)$$

$$T' = \sum_{i=0}^{\infty} T'^i \cos i\theta$$

where T^i and T'^i are the corresponding Fourier coefficients. The same Fourier harmonics used for the displacements are used for the temperature.

The temperature, T , for an element is assumed to be constant over each element in the meridional direction and have a step variation in the circumferential angle, θ . The variation is taken to be constant over an angle varying from θ_j to θ_{j+1} . Thus the Fourier coefficients T^i are given by

$$T^0 = \frac{1}{2\pi} \sum_j T_j (\theta_{j+1} - \theta_j) \quad (18)$$

$$T^i = \frac{1}{\pi} \sum_j T_j (\sin i\theta_{j+1} - \sin i\theta_j), \quad i > 0$$

Similar expressions are obtained for the Fourier coefficients involving temperature gradients.

In cases where the step variation in the circumferential direction is not considered accurate enough, the Fourier coefficients may be specified as initial information.

Thermal Strain Energy

The thermal strain energy U^t is given by

$$U^t = \int_v [\epsilon^t] [D] \{ \bar{\epsilon} \} dv \quad (19)$$

where

$$\{ \epsilon^t \} = \begin{Bmatrix} \epsilon_s^t \\ \epsilon_t^t \\ \epsilon_\theta^t \end{Bmatrix} = \begin{Bmatrix} \alpha_s T + \alpha_s T' z \\ \alpha_\theta T + \alpha_\theta T' z \end{Bmatrix}$$

$$[D] = \frac{1}{1 - v_{s\theta} v_{\theta s}} \begin{bmatrix} E_s & v_{s\theta} E_s \\ v_{\theta s} E_\theta & E_\theta \end{bmatrix} \quad (20)$$

$$\{ \bar{\epsilon} \} = \begin{Bmatrix} \bar{\epsilon}_s \\ \bar{\epsilon}_\theta \end{Bmatrix} = \begin{Bmatrix} \hat{e}_s + K_s z + \frac{1}{2} \hat{e}_{13}^2 \\ \hat{e}_\theta + K_\theta z + \frac{1}{2} \hat{e}_{23}^2 \end{Bmatrix}$$

The linear strains and rotations, \hat{e}_s , \hat{e}_θ , \hat{e}_{13} , \hat{e}_{23} , and the changes in curvature, K_s , K_θ are given in Ref. 4.

Substituting $[\epsilon^t]$, $[D]$ and $\{ \epsilon \}$ into Eq. 19 allows the thermal strain energy to be separated into two parts:

$$U^t = U_L^t + U_{NL}^t \quad (21)$$

where U_L^t is the thermal strain energy due to the linear strain-displacement relations and U_{NL}^t is the thermal strain energy due to nonlinearities in the strain-displacement relations. The linear and non-linear thermal strain energy expressions are given by

$$\begin{aligned}
 U_L^t = & \int \int [C_1(\alpha_s + v_{s\theta}\alpha_\theta) T \hat{e}_s + C_2(\alpha_\theta + v_{\theta s}\alpha_s) T \hat{e}_\theta \\
 & + D_1(\alpha_s + v_{s\theta}\alpha_\theta) T' K_s + D_2(\alpha_\theta + v_{\theta s}\alpha_s) T' K_\theta] r ds d\theta \quad (22)
 \end{aligned}$$

and

$$U_{NL}^t = \frac{1}{2} \int \int [C_1(\alpha_s + v_{s\theta}\alpha_\theta) T e_{13}^2 + C_2(\alpha_\theta + v_{\theta s}\alpha_s) T e_{23}^2] r ds d\theta \quad (23)$$

where α_s and α_θ are the coefficients of thermal expansion in the meridional and circumferential directions, respectively.

Thermal Loads due to Linear Strain Theory

For an element, the linear thermal loads for harmonic n may be written as a column matrix

$$\{Q_t^n\} = \left\{ \frac{\partial U_L^t}{\partial q^n} \right\} \quad (24)$$

and, using chain rule differentiation, may be converted to the partial derivatives with respect to the generalized coefficients, α , through the relation $\{\alpha\} = [A] \{q\}$ as given in Ref. 4. Thus,

$$\left\{ \frac{\partial U_L^t}{\partial q^n} \right\} = [A]' \left\{ \frac{\partial U_L^t}{\partial \alpha^n} \right\} \quad (25)$$

The problem reduces to the evaluation of the partial derivatives of U_L^t with respect to the coefficients, $\alpha_1, \alpha_2, \dots, \alpha_8$. These partial derivatives are obtained from Eqs. 22 of this paper and Eqs. 19 of Ref. 4.

For $i = 0$

$$\begin{aligned}
 \frac{\partial U_L^{t0}}{\partial \alpha_m^0} &= 2\pi [C_1(\alpha_s + v_{s\theta}\alpha_\theta) T^0 \int \frac{\partial e_s^0}{\partial \alpha_m^0} r ds \\
 &\quad + C_2(\alpha_\theta + v_{\theta s}\alpha_s) T^0 \int \frac{\partial e_\theta^0}{\partial \alpha_m^0} r ds \\
 &\quad + D_1(\alpha_s + v_{s\theta}\alpha_\theta) T'^0 \int \frac{\partial K_s^0}{\partial \alpha_m^0} r ds \\
 &\quad + D_2(\alpha_\theta + v_{\theta s}\alpha_s) T'^0 \int \frac{\partial K_\theta^0}{\partial \alpha_m^0} r ds] \tag{26}
 \end{aligned}$$

For $i > 0$

$$\begin{aligned}
 \frac{\partial U_L^{ti}}{\partial \alpha_m^i} &= \pi [C_1(\alpha_s + v_{s\theta}\alpha_\theta) T^i \int \frac{\partial e_s^i}{\partial \alpha_m^i} r ds \\
 &\quad + C_2(\alpha_\theta + v_{\theta s}\alpha_s) T^i \int \frac{\partial e_\theta^i}{\partial \alpha_m^i} r ds \\
 &\quad + D_1(\alpha_s + v_{s\theta}\alpha_\theta) T'^i \int \frac{\partial K_s^i}{\partial \alpha_m^i} r ds \\
 &\quad + D_2(\alpha_\theta + v_{\theta s}\alpha_s) T'^i \int \frac{\partial K_\theta^i}{\partial \alpha_m^i} r ds]
 \end{aligned}$$

The elements of $\{Q_t^n\}$ are listed in Appendix B.

Nonlinear Thermal Loads

The nonlinear thermal loads may be treated in the same manner as the generalized forces due to nonlinearities. The nonlinear thermal loads can be evaluated from the partial derivatives of U_{NL}^t with respect to the generalized displacements, q_1, q_2, \dots, q_8 .

$$\begin{aligned} \frac{\partial U_{NL}^t}{\partial q_m^n} = & \iint [c_1 (\alpha_s + v_{s\theta} \alpha_\theta) T \dot{e}_{13} \frac{\partial \dot{e}_{13}}{\partial q_m^n} \\ & + c_2 (\alpha_\theta + v_{\theta s} \alpha_s) T \dot{e}_{23} \frac{\partial \dot{e}_{23}}{\partial q_m^n}] r ds d\theta \end{aligned} \quad (27)$$

where n = harmonic number

$m = 1, 2, \dots, 8$.

With the same approximation as used in the evaluation of the generalized forces due to nonlinearities, the linear strain expressions are substituted in Eq. 27 and rearranged to yield

$$\begin{aligned} \frac{\partial U_{NL}^t}{\partial q_m^n} = & r_m L \sum_{i=0} \sum_{j=0} [c_1^{ijn} (\alpha_s + v_{s\theta} \alpha_\theta) T^j e_{13}^i \frac{\partial e_{13}^n}{\partial q_m^n} \\ & + c_2^{ijn} (\alpha_\theta + v_{\theta s} \alpha_s) T^j e_{23}^i \frac{\partial e_{23}^n}{\partial q_m^n}] \end{aligned} \quad (28)$$

where

$$T^j = \text{Fourier coefficients of temperature at time } t$$

The rotations and their derivatives with respect to the generalized displacements in Eq. 28 are evaluated approximately by using the finite difference relations described in the previous section (Equation 16).

The thermal effects have been incorporated into the computer program and checked for simple cases. However, a thorough evaluation of the thermal effects through numerical examples remains to be done.

Stress Resultants

In this research, the stress resultants were determined by the use of the assumed displacement functions and finite difference relations at the mid-point of each element.

The stress resultants for orthotropic shells are given by Ref. 4 as

$$\left[\begin{array}{c} N_s \\ N_\theta \\ N_{s\theta} \\ M_s \\ M_\theta \\ M_{s\theta} \end{array} \right] = \left[\begin{array}{cccccc} C_1 & v_{s\theta} C_1 & 0 & 0 & 0 & 0 \\ v_{\theta s} C_2 & C_2 & 0 & 0 & 0 & 0 \\ 0 & 0 & G_1 & 0 & 0 & 0 \\ 0 & 0 & 0 & D_1 & v_{s\theta} D_1 & 0 \\ 0 & 0 & 0 & v_{\theta s} D_2 & D_2 & 0 \\ 0 & 0 & 0 & 0 & 0 & G_2 \end{array} \right] \left[\begin{array}{c} \varepsilon_s \\ \varepsilon_\theta \\ \varepsilon_{s\theta} \\ K_s \\ K_\theta \\ K_{s\theta} \end{array} \right] \quad (29)$$

where $N_s, N_\theta, N_{s\theta}$ = stress resultants

$M_s, M_\theta, M_{s\theta}$ = moment resultants

The strains and curvatures in Eq. 29 are evaluated at the centers of the elements and given by

$$\begin{aligned}
 \epsilon_s &= \hat{\epsilon}_s + \frac{1}{2} \hat{\epsilon}_{13}^2 - e_s^t \\
 \epsilon_\theta &= \hat{\epsilon}_\theta + \frac{1}{2} \hat{\epsilon}_{13}^2 - e_\theta^t \\
 \epsilon_{s\theta} &= \hat{\epsilon}_{s\theta} + \hat{\epsilon}_{13} \hat{\epsilon}_{23} \\
 K_s &= - \frac{\partial \hat{\epsilon}_{13}}{\partial s} - K_s^t \\
 K_\theta &= - \frac{1}{r} \left[\frac{\partial \hat{\epsilon}_{23}}{\partial \theta} + \hat{\epsilon}_{13} \sin\phi \right] - K_\theta^t \\
 K_{s\theta} &= - \frac{1}{r} \frac{\partial \hat{\epsilon}_{13}}{\partial \theta} + \frac{\sin\phi}{r} \hat{\epsilon}_{23} - \frac{\partial \hat{\epsilon}_{23}}{\partial s}
 \end{aligned} \tag{30}$$

where e_s^t , e_θ^t , K_s^t and K_θ^t are the strains and changes in curvature due to thermal loads, and given by

$$\begin{aligned}
 e_s^t &= \alpha_s \sum_{i=0} T^i \cos i\theta \\
 e_\theta^t &= \alpha_\theta \sum_{i=0} T^i \cos i\theta \\
 K_s^t &= \alpha_s \sum_{i=0} T'^i \cos i\theta \\
 K_\theta^t &= \alpha_\theta \sum_{i=0} T'^i \cos i\theta
 \end{aligned} \tag{31}$$

In the computer code, the partial derivatives of the rotations with respect to s are evaluated approximately by using finite difference relations. Using finite difference relations, the changes in curvature are evaluated as

$$\begin{aligned}
 K_s &= \sum_{i=0} k_s^i \cos i\theta \\
 K_\theta &= \sum_{i=0} k_\theta^i \cos i\theta \\
 K_{s\theta} &= \sum_{i=0} k_{s\theta}^i \sin i\theta \\
 k_s^i &= \frac{q_4^i - q_8^i}{L} - \alpha_s T'^i
 \end{aligned} \tag{32}$$

$$\begin{aligned}
 k_\theta^i &= -\frac{1}{r_m} [ie_{23}^i + e_{13}^i \sin\phi_m] - \alpha_\theta T'^i \\
 k_{s\theta}^i &= \frac{1}{r_m} [ie_{13}^i + \sin\phi_m e_{23}^i + i \frac{\bar{q}_7^i - \bar{q}_3^i}{L} - \frac{i \sin\phi_m (\bar{q}_7^i + \bar{q}_3^i)}{2}] \\
 &\quad + \cos\phi_m \frac{q_6^i - q_2^i}{L} - (\phi'_m + \frac{\cos\phi_m}{r_m}) \sin\phi_m \frac{q_6^i + q_2^i}{2}
 \end{aligned}$$

where $\bar{q}_7^i = -q_5^i \sin\phi_L + q_7^i \cos\phi_L$

$$\bar{q}_3^i = -q_1^i \sin\phi_o + q_3^i \cos\phi_o$$

$$\phi' = \frac{d\phi}{ds}$$

The shear resultants are determined approximately from the equations of equilibrium of the undeformed shell as

$$\begin{aligned} Q_s &= \frac{1}{r} \left[\frac{\partial}{\partial s} (rM_s) + \frac{\partial M_{s\theta}}{\partial s} - M_\theta \sin\phi \right] \\ Q_\theta &= \frac{1}{r} \left[\frac{\partial}{\partial s} (rM_{s\theta}) + \frac{\partial M_\theta}{\partial s} + M_{s\theta} \sin\phi \right] \end{aligned} \quad (33)$$

These shear resultants at the nodes are obtained by using the finite difference relations except for the first and last nodes as

$$\begin{aligned} Q_s(J) &= \frac{1}{r_{av}} \left\{ \frac{1}{L_{av}} [r_m(J) M_s(J) - r_m(J-1) M_s(J-1)] + \frac{1}{2} \left[\frac{\partial M_{s\theta}(J)}{\partial \theta} + \frac{\partial M_{s\theta}(J-1)}{\partial \theta} \right. \right. \\ &\quad \left. \left. - \frac{\sin\phi_{av}}{2} [M_\theta(J) + M_\theta(J) + M_\theta(J-1)] \right] \right\} \\ Q_\theta(J) &= \frac{1}{r_{av}} \left\{ \frac{1}{L_{av}} [r_m(J) M_{s\theta}(J) - r_m(J-1) M_{s\theta}(J)] + \frac{1}{2} \left[\frac{\partial M_\theta(J)}{\partial \theta} + \frac{\partial M_\theta(J-1)}{\partial \theta} \right] \right. \\ &\quad \left. + \frac{\sin\phi_{av}}{2} [M_{s\theta}(J) + M_{s\theta}(J-1)] \right\} \end{aligned} \quad (34)$$

$$\text{where } r_{av} = \frac{1}{2}[r_m(J) + r_m(J-1)]$$

$$L_{av} = \frac{1}{2}[L(J) + L(J-1)]$$

$$\phi_{av} = \frac{1}{2}[\phi_m(J) + \phi_m(J-1)]$$

$$J = 2, 3, \dots \text{number of element}$$

METHODS OF SOLUTION

The numerical methods of solution which have been used in DYNASOR II to calculate the nodal displacements of the shells under study are discussed in this section. Three independent methods have been utilized with one of the methods being varied to provide a total of five different numerical solution schemes. The formulation of these methods for use in solving the shell equations is presented and the results obtained using each method are discussed. Additional methods of solution are to be evaluated and the results presented in Ref. 25.

The equations of motion, Eq. 2, can be reduced to a system of equations of the form

$$[M] \ddot{\{q\}} + [K] \dot{\{q\}} = \{F(t,q)\} \quad (35)$$

The load matrix, $\{F(t,q)\}$, is equivalent to the right-hand side of Eq. 2. The numerical schemes discussed are formulated to satisfy these governing differential equations of motion.

Since a closed-form solution of Eq. 35 is generally not available, a numerical method must be used to determine the response of the shell. The numerical methods employed calculate the displacements for any time, t , increment the time by an amount Δt , and then solve for the displacements at the new time, $t + \Delta t$. This step-by-step calculation of the displacements must be performed for a large number of time increments in order to determine the response characteristics of the shell of revolution.

In order to start the numerical solution of Eq. 35, the initial displacements and velocities of the nodes of the shell must be known. These initial conditions are specified in the form

$$\begin{aligned} q_0 &= \{q\}_0 \\ \text{and} \\ \dot{q}_0 &= \{\dot{q}\}_0 \end{aligned} \tag{36}$$

Although a few of the numerical methods of solution use the same procedure for calculating the response at each time step, most solution schemes require the development of special procedures for calculating the displacements at the end of the initial step. The method of starting each of the solution schemes is presented.

The accuracy and stability of the numerical solution schemes as well as the computer time required to obtain the responses are investigated. An efficient scheme should provide a solution which remains numerically stable for large time increments. The scheme should also be able to determine accurately the response characteristics of the shell without the expenditure of large amounts of computer time. The relative amounts of computer storage space required by the various numerical schemes are also discussed. The accuracies inherent in the different methods are presented and the effect of truncation errors upon the value of the displacements is discussed.

Levy and Kroll,²⁶ investigated both the accuracy and convergence of numerical integration methods. These methods were used to determine the dynamic responses of single-degree-of-freedom and multi-degree-of-freedom structures to impact loads. A central difference pattern was used to replace

the acceleration term in the equations of motion and Houbolt's method of solution was applied. It was concluded that the Houbolt method was the only method tested which gave convergent results for large time increments but that errors introduced by using these large time steps caused a damping out of the system response. It was also concluded that "all the methods give good results when the time increment is less than about 1/30 of the period of the highest frequency mode."

Using a finite difference formulation, Johnson and Greif²⁷ have presented the results of linear dynamic response studies of cylindrical shells. These results were obtained by the direct application of two different methods of timewise numerical integration. An explicit method and an implicit (Houbolt) method are used with the relative merits of each method being discussed. For the explicit solution, a central difference expression is used to approximate the accelerations of the mesh points. The time increment used in the explicit solution must be chosen small enough to insure the numerical stability of the solution. Stability criteria based upon physical considerations are developed and used to evaluate the critical ratio of the time and spatial increments. A damping effect upon output quantities was noted for solutions using Houbolt's method with large time increments. It was reported that "the time increment has to be smaller than about 1/50th of the period of a particular mode of vibration in order that important output quantities in that particular mode not be significantly damped." It is warned that unless that criterion is adhered to, the Houbolt method will have a tendency to damp out the motion of the higher modes of vibration. The explicit method did not exhibit this damping

phenomenon. Both methods were shown to give the same results. After considering the relative efficiencies of both methods measured in terms of the amount of computer time necessary for the accurate solution of a given problem, it was concluded that the explicit method is more efficient for determining rapidly varying responses, but for the determination of slower responses the Houbolt scheme becomes more efficient.

A finite difference formulation for the nonlinear dynamic response of thin-shell structures has been presented by Wrenn, Sobel and Silsby.¹¹ Three numerical methods are used to solve the equations of motion of the system and the stability and convergence of each method is examined. An explicit finite difference expression, the same expression as that used by Johnson and Greif, is used to represent the accelerations of the mesh points. In addition, two numerical integration schemes, the Runge-Kutta method and the Adams-Moulton predictor-corrector method, are examined. The conclusion is reached that, "In most cases, the 'critical time step' is so small that the larger truncation error of the finite difference method does not create a serious accuracy problem." Thus, it is concluded that the critical time increment for stability, not the truncation error, is a governing factor in the finite difference procedure. Several procedures for determining this "critical time step" are presented and discussed. Based upon work with a right circular cylinder, Wrenn, Sobel and Silsby also conclude that, of the three methods tested, the explicit finite difference procedure is the most efficient.

Houbolt's Method

The finite difference method of solution developed by Houbolt²² for use in dynamic structural response studies of aircraft can be adapted for use in determining the dynamic nonlinear response of shells of revolution. The accelerations in Eq. 35 are replaced by a finite difference approximation of the second derivative. This substitution allows development of recurrence relations which can be used for the step-by-step calculation of the displacements of the shell.

The accelerations of the nodes of the shell are approximated by the third order backwards difference expression

$$\{\ddot{q}_{n+1}\} = \frac{1}{(\Delta t)^2} \{2q_{n+1} - 5q_n + 4q_{n-1} - q_{n-2}\} \quad (37)$$

The accuracy of this representation is of the order $(\Delta t)^2$.

Substituting Eq. 37 into Eq. 35 and simplifying yields

$$(2[M] + (\Delta t)^2[K]) \{q_{n+1}\} = (\Delta t)^2 \{F(t, q)_{n+1}\} + [M] \{5q_n - 4q_{n-1} + q_{n-2}\} \quad (38)$$

This equation is valid for all time increments but must be modified for the first step since the values of $\{q_{-2}\}$ and $\{q_{-1}\}$ are not known. This occurrence is common when solving initial value problems by finite difference procedure and merely requires that a method be developed to start the solution. Equation 38 will, however, be used to calculate the displacements for all time increments except the first.

To start the solution, assume

$$\{\dot{q}_o\} = \frac{1}{6\Delta t} \{2q_1 + 3q_o - 6q_{-1} + q_{-2}\} \quad (39)$$

and

$$\{\ddot{q}_o\} = \frac{1}{(\Delta t)^2} \{q_1 - 2q_o + q_{-1}\} \quad (40)$$

The initial accelerations are obtained using Eq. 35 evaluated at $t = 0$ which gives

$$[M] \{\ddot{q}_o\} = \{F(0, q_o)\} - [K] \{q_o\} \quad (41)$$

Rearranging Eq. 40 gives

$$\{q_{-1}\} = (\Delta t)^2 \{\ddot{q}_o\} + \{2q_o - q_1\} \quad (42)$$

By combining Eqs. 39 and 42 an expression for $\{q_{-2}\}$ is developed

$$\{q_{-2}\} = 6(\Delta t)^2 \{\ddot{q}_o\} + 6(\Delta t) \{\dot{q}_o\} + 9\{q_o\} - 8\{q_1\} \quad (43)$$

Substituting Eqs. 42 and 43 into Eq. 38 for the first time increment ($n=0$) and approximating the forces at the end of the first time step by the forces at time, $t = 0$, provides an expression in terms of the initial displacements, velocities and accelerations which can be solved to get $\{q_1\}$

$$(6[M] + (\Delta t)^2 [K]) \{q_1\} = (\Delta t)^2 \{F(0, q_o)\} + [M] \{2(\Delta t)^2 \ddot{q}_o + 6\Delta t \dot{q}_o + 6q_o\} \quad (44)$$

This equation is used to determine the displacement at the end of the first time step. Using Eq. 42, a fictitious matrix of displacements, $\{q_{-1}\}$ can be determined. The displacements are then available so Eq. 38 can be used for each subsequent time step.

Chan, Cox and Benfield Method

Chan, Cox, and Benfield²⁰ developed a numerical method of solution which can be applied to multi-degree-of-freedom structures subjected to dynamic loads. A recurrence matrix of finite differences is derived which can be used for the step-by-step calculation of the dynamic response of the idealized structures. The method is actually a special case of the more general procedure presented by Newmark.²⁸

The numerical solution of the differential equations of motion for the dynamic system is accomplished by replacing the derivatives by the following finite difference equivalents

$$\{\dot{q}_{n+1}\} = \{\dot{q}_n\} + \frac{\Delta t}{2} \{\ddot{q}_{n+1} + \ddot{q}_n\}$$

and

(45)

$$\{q_{n+1}\} = \{q_n\} + \Delta t \{\dot{q}_n\} + (\frac{1}{2} - \beta) (\Delta t)^2 \{\ddot{q}_n\} + \beta (\Delta t)^2 \{\ddot{q}_{n+1}\}$$

The parameter of generalized acceleration, β , expresses the acceleration within a time interval in terms of the initial and final accelerations of the interval. As reported in Ref. 20, "the value of β can be anywhere between 0 and 1/4" with the choice of this parameter depending upon "the physical characteristics of the system, accuracy desired, and certain limits of application."

Setting the value of β equal to 1/4 corresponds to using trapezoidal integration formulas to determine both the displacements and velocities of the system. The trapezoidal integration procedure is consistent with the assumption that a constant acceleration, equal to the mean value of the initial and final accelerations of the increment, exists within the interval.

By applying Simpson's one-third rule to integrate the accelerations and the trapezoidal formulas to integrate the velocities, the equation corresponding to $\beta = 1/6$ can be derived. This expression is consistent with assuming a linear variation of the acceleration within each step.

The Chan, Cox, and Benfield solution corresponds to a second order central difference pattern when the value of the generalized acceleration parameter, β , is zero.

Eliminating the matrix of damping coefficients from the equations in Ref. 20 the displacements for the $(n+1)$ th time step can be calculated from the expression

$$[A] \{q_{n+1}\} = [B] \{q_n\} - [A] \{q_{n-1}\} + \beta(\Delta t)^2 \{F_{n+1} + (\frac{1}{\beta} - 2)F_n + F_{n-1}\} \quad (46)$$

where

$$[A] = [M] + \beta(\Delta t)^2 [K]$$

$$[B] = 2[M] - (1-2\beta)(\Delta t)^2 [K]$$

Equation 46 is used to calculate the displacements at the end of each increment except the first one.

Since Eq. 46 requires the knowledge of the displacements at the end of two previous time steps, a special procedure must be used to calculate the displacements at the end of the first increment. Again, by simplifying the equations of Ref. 20 the equations to calculate the displacements at the end of the first increment become

$$[A] \{q_1\} = [C] \{q_0\} + \Delta t [M] \{\dot{q}_0\} + \beta(\Delta t)^2 \{F(t_1, q_1)\} + (\frac{1}{2}-\beta)(\Delta t)^2 \{F(0, q_0)\} \quad (47)$$

where

$$[C] = [M] - (\frac{1}{2}-\beta)(\Delta t)^2 [K].$$

Runge-Kutta Method

For the special second-order system of differential equations where the accelerations are not a function of the velocities of the system, we have

$$\{\ddot{q}\} = G(t, q) \quad (48)$$

These accelerations are calculated using Eq. 35. For this system of equations the general fourth-order forward integration Runge-Kutta formulas taken from Hildebrand²⁹ reduce to

$$\{q_{n+1}\} = \{q_n\} + \Delta t \{\dot{q}_n\} + \frac{\Delta t}{6} \{m_0 + m_1 + m_2\} + O(\Delta t^5) \quad (49)$$

$$\{\dot{q}_{n+1}\} = \{\dot{q}_n\} + \frac{1}{6} \{m_0 + 2m_1 + 2m_2 + m_3\} + O(\Delta t^5) \quad (50)$$

where

$$\begin{aligned} \{m\}_0 &= \Delta t G(t_n, \{q_n\}) \\ \{m\}_1 &= \Delta t G(t_n + \frac{\Delta t}{2}, \{q_n + \frac{\Delta t}{2} \dot{q}_n\}) \\ \{m\}_2 &= \Delta t G(t_n + \frac{\Delta t}{2}, \{q_n + \frac{\Delta t}{2} \dot{q}_n + \frac{\Delta t}{4} m_0\}) \\ \{m\}_3 &= \Delta t G(t_n + \Delta t, \{q_n + \Delta t \dot{q}_n + \frac{\Delta t}{2} m_1\}) \end{aligned} \quad (51)$$

The Runge-Kutta method of solution offers many advantages (Ref. 29) over other numerical schemes:

1. The formulas are the same for each stage of the calculation and do not require any special starting procedures for the first increments.

2. The spacing may be changed at any interval during the solution since this method does not require information from previous stages.
3. Runge-Kutta methods can be used to obtain accurate results [the truncation error in a fourth-order Runge-Kutta solution is of order $(\Delta t)^5$].

An inherent disadvantage of this method is that for each stage of the advancing calculation, four calculations of the accelerations are necessary. In order to be competitive with other numerical solution routines the critical time increment for the Runge-Kutta method must therefore be substantially larger (preferably by a factor of at least 4) than the step allowed by other methods.

Approximation of Loads Matrix

Both the method of Houbolt and the Chan, Cox, and Benfield method require that the loads at the end of the nth time increment be known in order to calculate the displacements at the end of that increment. These loads, because of the presence of the nonlinear terms, are a function of the displacements which are to be calculated. It is therefore not possible to evaluate these terms exactly.

Consequently, the right-hand side of Eq. 35 will be evaluated using a first order Taylor's series expanded about the nth time increment.

$$\{F(t, q)_{n+1}\} = \{F(t, q)_n\} + \{\frac{\partial}{\partial t} \{F(t, q)_n\} \Delta t + O(\Delta t)^2\} \quad (52)$$

Approximating the partial derivative by a first order backwards difference expression gives

$$\{F(t, q)_{n+1}\} \approx 2\{F(t, q)_n\} - \{F(t, q)_{n-1}\} \quad (53)$$

This expression has an inherent error of order $(\Delta t)^2$ which is the same as the order of accuracy inherent in both the Houbolt and the Chan, Cox, and Benfield solutions. It corresponds to a linear extrapolation of the loads at the two previous time increments.

Using a second order expression the loads may be approximated to an accuracy of order $(\Delta t)^3$ by

$$\{F(t, q)_{n+1}\} \approx 3\{F(t, q)_n\} - 3\{F(t, q)_{n-1}\} + \{F(t, q)_{n-2}\} \quad (54)$$

It is assumed when using this expression that by passing a parabola through the loads at the three previous time increments the loads for the nth time increment can be determined.

Numerical Results

The results obtained using the various methods of solution are evaluated to determine the method of solution most advantageous for the DYNASOR II program. The numerical stability of each method is investigated and an extremely thorough test of the Houbolt solution scheme is made after concluding that this seems to be the most promising method of solution.

Runge-Kutta Evaluation

A shallow spherical cap with clamped edges was analyzed using the Runge-Kutta method of solution. The cap was subjected to an instantaneously applied (at time = 0) internal pressure of 70 psi. Only the zero harmonic response was determined. Thirty elements were used giving a total of 124 degrees of freedom.

Linear solutions of the problem were numerically unstable for time increments of 2.0×10^{-6} , 1.0×10^{-6} , and 0.5×10^{-6} seconds. This instability consistently occurred after only a few time steps had been taken. The time increment was further reduced to the very small value of 0.5×10^{-8} seconds and the solution obtained did not exhibit any numerical instability. Utilizing this extremely small time increment would require prohibitive amounts of computer time to determine the response of a shell.

Since for an initial value problem, the accuracy of the displacements of the initial steps greatly affects the numerical stability of the solution, a smaller time increment used during the initial steps can possibly improve the stability of the solution. DYNASOR II was modified to use an increment over the initial steps which was several times smaller than the input step size. After completing these initial steps, the input time increment was used for the remaining steps. This approach did provide additional stability by increasing the allowable time step to 0.5×10^{-7} seconds. It is presumed that the critical time increment would have been decreased by the inclusion of the nonlinear terms.

From these results, it can be concluded that the advantages afforded by the simplicities of application and the accuracy of the Runge-Kutta method are more than offset by the small critical time increment which is required when this method is applied to dynamic shell of revolution problems. Utilizing this method of solution therefore requires unreasonably large amounts of computer time to determine the response of a shell.

Chan, Cox, and Benfield Solution ($\beta = 1/6$ and $\beta = 0$)

For a variety of problems, attempts were made to calculate the response curves using both $\beta = 0$ and $\beta = 1/6$. A numerically stable solution was never obtained using time steps as small as 0.1×10^{-6} seconds. The results obtained using the Runge-Kutta solution suggest that by reducing the time step even further a stable solution could possibly have been obtained. These small time increments were not used since the amount of computer time required to obtain a solution to a problem would render the method impractical.

Houbolt Method vs. Chan, Cox, and Benfield Routine with $\beta = 1/4$

To determine the most advantageous numerical method of solution for use in DYNASOR II, a comparison was made of the responses obtained using the method of Chan, Cox, and Benfield ($\beta = 1/4$) and Houbolt's method. The shell selected to serve as a test problem for the two numerical methods is shown in Fig. 7. This cap-torus-cylinder configuration was subjected to a 50 psi internal pressure. The shell was idealized using 50 elements distributed so that a large number of elements were concentrated in the vicinity of the cap-torus intersection and near the torus-cylinder intersection. With this element distribution, the size of the elements varies extensively. The widely varying element sizes coupled with the irregular shape of the shell provide a real and critical test of the numerical methods.

Using the zero harmonic, the displacements and stresses are calculated utilizing both numerical methods with single-precision numerical accuracy. By considering the results presented in Fig. 7, it can be

concluded that the displacements calculated using both numerical methods are almost identical. The stresses calculated at the cap-torus intersection are presented in Figs. 8 and 9. Excellent agreement between the values calculated by the two methods is once again noted.

Since the displacements and stresses calculated by both numerical methods of solution are essentially the same, the choice of the most advantageous method of solution can be made based upon economic considerations. The largest time increment which can be used for this problem by the Chan, Cox, and Benfield method is 1×10^{-6} second. Houbolt's method of solution is, however, stable for a time increment of 3×10^{-6} seconds. Obviously, a tremendous saving of computer time can be realized by using the numerical method of solution which utilizes the larger time step. In addition, the amount of computation time required per step is less for the Houbolt scheme than for the Chan, Cox, and Benfield routine. This can be explained by comparing Eqs. 38 and 46. For each time step, two matrix multiplications must be performed using the Chan, Cox, and Benfield scheme but only one multiplication is necessitated by the Houbolt procedure. This saving of computer time becomes increasingly more important as the number of finite elements used is increased. The combined effect of using the larger time step and decreasing the computer time per step is to provide a solution of this problem almost four times faster using Houbolt's method. For several of the analyses presented in the application section, the same advantage was noted using Houbolt's solution.

By considering Eqs. 38 and 46 it can be seen that the amount of computer storage space required for the Houbolt scheme is slightly greater than the space required for the Chan, Cox, and Benfield procedure. This results from the necessity of retaining the displacements at three previous increments for Houbolt's solution. The Chan, Cox, and Benfield procedure requires that the displacements at only two previous steps be retained. This slight disadvantage of requiring additional storage space is more than offset by the many advantages and benefits to be accrued by using the Houbolt solution scheme.

Test Problem for Houbolt Solution Scheme

The problem selected to serve as a critical test of the Houbolt method of solution is the shallow spherical cap ($\lambda = 6$) with clamped edges depicted in Fig. 10. The geometric and material properties presented at the top of this figure are used throughout the analysis. The cap is excited by an instantaneously applied load which is concentrated at the apex of the shell.

This particular problem was selected for two reasons. First, the problem is highly nonlinear. The high degree of nonlinearity can be established by looking at the static load-deflection curve (Fig. 10) for this shell. The results were obtained by the method described in Ref. 4 using the Newton-Raphson method of solution and are in agreement with the results presented by Mescall³⁰ and Bushnell.³¹ A forty pound load was selected for use in the dynamic test case. For this loading,

the displacements predicted by a nonlinear analysis are more than four times larger than the displacements predicted by a linear analysis. Hence, a highly nonlinear problem is to be solved.

Second, the singularity which exists at the apex of this shell gives rise to extremely large terms in the structural stiffness matrix. The corresponding terms in the mass matrix are rather small. The net effect of a large stiffness to mass ratio is to give a speed of sound in the element which is very large. Since some of the stability criteria developed in the finite difference approach (Ref. 11, 14, and 27) are based upon the time required for a signal to travel from one mesh point to another, applying these criteria to this problem results in the prediction of an extremely small time increment. The same effect is produced by using very small elements.

Numerical Accuracy

The effect of using a greater degree of numerical accuracy in the solution of this highly nonlinear problem was investigated. The DYNASOR programs were used on an IBM 360/65 computer with both single-precision (7 significant figures) and double-precision (16 significant figures) numerical accuracy. A time increment of 0.125×10^{-6} seconds was used with the shell being idealized by thirty finite elements.

A comparison of the single-precision and double-precision solutions can be made by considering Fig. 11. A slight decrease in both the period and amplitude of the predicted motion is noticed in the single precision results.

The response curves for several shells in which the behavior is only moderately nonlinear are discussed in the applications section. These curves, obtained using single precision accuracy in the DYNASOR programs, are shown to be in quite good agreement with the solutions to which they are being compared. This implies that the double-precision accuracy is necessary in the 360/65 system only for the analysis of shells which exhibit highly nonlinear behavior. It is believed that if the DYNASOR programs are used on computers which have a longer word length than the 360/65 system double-precision accuracy will not be necessary.

Effect of Load Extrapolation Procedure

The effect of the accuracy of the extrapolation procedure used to determine the loads matrix in Eq. 35 was also investigated. Again, a thirty element idealization of the shallow cap was used along with a time increment of 0.125×10^{-6} seconds. By evaluating the results presented in Fig. 12, it can be concluded that even for highly nonlinear problems, there is almost no advantage accrued by using a parabolic rather than a linear extrapolation procedure. For a time increment of 0.25×10^{-6} seconds, the solution became numerically unstable using the cubic extrapolation procedure but remained stable for the linear approximation. Because of this added stability, it is concluded that a linear extrapolation procedure can be effectively used to approximate the loads at the nth time increment. Using this linear procedure rather than the parabolic one reduces the amount of storage space required by the program and also slightly reduces the run time required for a problem since fewer calculations have to be performed for each increment.

Convergence with Improved Finite Element Idealization

As the finite element idealization of a shell is improved, the displacements calculated using any acceptable method should converge. To show that the solutions obtained using the Houbolt method in the DYNASOR programs do converge, the shell depicted in Fig. 10 was analyzed using 15, 30 and 50 element representations. The element distribution was chosen so that the elements were concentrated at the apex and at the supports of the shell where the displacements and stresses vary rapidly.

Since linear displacement functions are assumed for the variables in the nonlinear strain energy expression and since strip integration is used across the element, it would be expected that the convergence of the solution by increasing the number of finite elements would be rather slow. This is not the case, however, since a comparison of the results presented in Fig. 13 shows that the response curves obtained using the 30 and 50 element idealizations are practically identical but that the solution has not completely converged for the 15 element representation. The response calculated for the 15 element representation seems accurate enough for many engineering purposes since only the period and not the amplitude of the motion appears changed.

Each element used in the representation of the shell increases the size of the matrices which must be manipulated and hence increases, by four, the number of equations to be solved for each time increment. This results in a substantial increase in computation time per step. For the zero harmonic the 50 element case required more than three times the

amount of computer time necessary for the 15 element example (0.0067 minutes/step compared to 0.0021 minutes/step).

Effect of Time Increment Variation

Houbolt's method has been shown (Ref. 26 and 27) to exhibit a damping phenomenon for large values of the time increment. It is necessary, therefore, to show that the time increment used to obtain a solution is small enough so that the damping inherent in the solution scheme does not affect the calculated response. Using double-precision accuracy and again employing a thirty element idealization of the cap, the apex displacements that were calculated using two different time increments (0.25×10^{-6} and 0.125×10^{-6} seconds) are presented in Fig. 14. By considering this figure, it can be seen that the solution has converged for a time increment as large as 0.25×10^{-6} seconds. The Houbolt solution, however, becomes numerically unstable with a time step of 0.5×10^{-6} seconds because of the influence of the nonlinear terms. The Chan, Cox, and Benfield solution ($\beta = 1/4$) was numerically unstable for a time step as small as 0.125×10^{-6} seconds. Hence, it is again observed that the Houbolt solution scheme is numerically stable for much larger time steps than can be used in the Chan, Cox, and Benfield routine.

The response of the shell depicted in Fig. 10 subjected to a uniform external pressure is presented in the applications section. A time step of 1×10^{-6} seconds was used to calculate this response. Since the response to the pressure loading does not exhibit the high degree of nonlinearity present under the concentrated loading, a larger time increment could be used. These results indicate that the critical

time increment which can be used depends not only upon the geometry of the shell but also upon the degree of nonlinearity.

APPLICATIONS

The purpose of this section is:

- (1) To present a comparison of current findings with other theoretical and experimental results.
- (2) To present solutions to problems that will demonstrate the capabilities of the computer code.

The first example employs the shallow shell and the axisymmetric loading described by Klein and Sylvester.¹⁹ The results have been verified by Popov using the normal mode superposition technique.

The shell had a radius of curvature of 22.27 inches, base diameter of 20 inches, a shell rise of 2.37 inches, and a thickness of 0.41 inches. The modulus of elasticity and Poisson's ratio were taken to be 10.5×10^6 psi and 0.3, respectively and the ends of the shell were assumed to be fixed.

Klein and Sylvester present a linear analysis based on conical frustum elements and the numerical integration scheme described in Ref. 20. The formulation also makes use of a mass matrix based on energy principles but does not include the effects of rotary inertia. These effects are not significant for the problem under consideration. The time step of 1×10^{-5} seconds and the 30 element idealization used in Ref. 19 were used in this research.

An investigation of Fig. 15 reveals that the agreement is quite good and the effect of nonlinearities is not significant. The slight discrepancies at the higher times can conceivably be attributed to the differences in formulation and method of solution or the fact that double precision arithmetic is employed by Klein and Sylvester.

The second example involves the cylindrical shell described in Ref. 27 having geometric and material properties typical of those used in the missile industry. The structure is subjected to a blast loading and requires the use of the 0, 1, and 2 Fourier harmonics. Figure 16 shows a plot of the time history of the Fourier coefficients of normal displacement at the free end of the cylinder. The results obtained are identical to the ones presented in Ref. 27. Houbolt's solution procedure with a time increment of 5×10^{-6} seconds was used in the solution.

The third example illustrates the versatility of the computer code and solves the important problem of the symmetric buckling of shallow spherical caps under a step pressure loading. The problem has been investigated by other researchers^{32, 33, 34} and most results are now in good agreement. However, at the beginning of this study only the results of Huang³³ and Simitses³² were available and they did not agree.

The shell selected for the study is the one studied experimentally in Ref. 35 with different values of the shallow shell parameter being obtained by varying the thickness. The results are depicted in Fig. 17. The current results were obtained by using 30 elements and the numerical integration scheme presented in Ref. 20 with $\beta = \frac{1}{4}$; however, a check has been made using Houbolt's method and the results are the same.

This problem again reveals the advantages of the Houbolt's method over the method of Chan, Cox, and Benfield with $\beta = \frac{1}{4}$. The solution obtained with Houbolt's method used a time increment of 1×10^{-6} seconds whereas the method of Chan, Cox and Benfield required a time increment of $.125 \times 10^{-6}$ seconds. Thus, for this problem Houbolt's method is more than eight times as efficient as the method of Ref. 20.

The curves shown in Fig. 17 reveal that the results obtained with DYNASOR and those presented in Refs. 33 and 34 are in good agreement. A more detailed discussion of this problem is given in Ref. 21.

The fourth application of the program concerns the solution of a problem that has never been solved. This problem is the one of asymmetrical buckling of a shallow cap under a step pressure loading. The shell used in the study has the same basic geometry as the one used in the third example but has a thickness corresponding to a shallow shell parameter λ , of 6.

The response of four Fourier harmonics was investigated by both Houbolt's method and the method of Ref. 20 and the results were the same. In one case the 0, 1, and 2 harmonics were used and in the second case the 0, 2, and 3. Both cases revealed that for the case of $\lambda = 6$, there is no build up in the first or third Fourier harmonics and it is the second harmonic that reaches relatively large displacements. The same phenomenon has previously been observed in the static case.

The loading consisted of a constant uniform step pressure over the entire shell except for a slight increase over a circumferential angle of four degrees. It was necessary to do this in order to excite the first, second and third Fourier harmonics.

Figure 18 depicts the response of the second harmonic for various pressure ratios and shows how a relatively small increase in the load can significantly increase the response of the second harmonic when a critical loading is approached. Figure 19 shows how the displacements for the second harmonic can build up to values having the same order of magnitude of those of the symmetric component and at some critical time

the two combine to give a very large displacement and enable us to define a buckling load.

The dynamic buckling pressure may be obtained from Fig. 19. It is seen from this figure that buckling occurs at $P/P_{cr} = .604$ as compared with .64 for symmetrical buckling. However, it is observed from Fig. 19 that the second harmonic is excited appreciably for all values of P/P_{cr} above .5. Thus, the threshold value is .5. This threshold value has not been shown to be a buckling load but it is conceivable that if the calculations were carried for a large enough period of time buckling might occur. At most, the use of the threshold value is slightly conservative. The possibility of asymmetrical buckling is depicted in Fig. 17 as any value above $P/P_{cr} = .5$.

The fifth example (Fig. 20) demonstrates the feasibility of the finite element method for the analysis of wave propagation in shells of revolution. This example solves the problem of a cylindrical bar having a length of 24 inches, radius of 6 inches, and a wall thickness of 0.1 inches. The modulus of elasticity, Poisson's ratio and the mass density were taken as 10×10^6 psi, 0.333, and 0.0942 lbm/in^3 , respectively. The cylinder was assumed to be fixed at one end and free at the other with the free end being subjected to a uniformly distributed axial pressure of infinite duration having a value of 100 psi. The solution was performed using Houbolt's method in double precision arithmetic, a time increment of 1×10^{-6} seconds, and 50 finite elements. The element breakdown was 10 of .24" in length, 10 of .48", 10 of .96", 10 of .48", and 10 of .24" in length.

The exact solution is obtained from elementary wave mechanics. The speed of sound in the material is given by

$$v_c = \sqrt{\frac{E}{(1-\nu^2)\rho}} \quad (55)$$

Substituting the material properties into Eq. 55 yields a speed of sound of 214,749 in/sec. Thus, an expansion wave travels down the cylinder at the prescribed speed. The theoretical stress behind the wave is 100 psi with zero stress existing in front of the wave. When the wave reaches the wall it is reflected as an expansion wave which travels back down the cylinder. After the time required for the wave to transverse the cylinder in both directions the state of stress is a constant value of 200 psi. The expansion wave is reflected from the free end as a compressive wave which reduces the stress to 100 psi and back to zero after reflection from the fixed end. This behavior gives displacement of a saw tooth nature as shown in Fig. 20 along with the finite element results. It is noted that the agreement is excellent.

Figures 21 and 22 present the displacements and meridional stress along the length of the cylinder after 50 microseconds. After this period of time, the wave has travelled through the two changes in length in the finite element idealization. It is noted that the finite element and wave theory results are in excellent agreement for displacement and quite good for stresses.

The solution of the sixth example problem was performed for the purpose of checking out the code for multiple harmonics. The shell

selected for this example was a spherical cap with a radius of curvature of 60 inches, a base radius of 4.28 inches, and a thickness of 0.125 inches. The loading was localized as shown in Fig. 23 and was applied over a two-inch radius circle with the center 3° from the apex. The solution was obtained using twenty-eight elements and the first five Fourier harmonics. The method of Ref. 20 with a time increment of $.25 \times 10^{-6}$ seconds was used in the solution.

Figure 23 is a plot of the vertical deflection of $\theta = 0^\circ$ and $r = 1.56$ inches and reveals that the dynamic solution oscillates about the static solution. Next to the zero harmonic, the first Fourier harmonic was found to give the most significant contribution. The lower displacement peak that is experienced at a time of approximately 1000 μsec is due to the fact that the zero and the first harmonics are out of phase.

Figures 24 through 27 represent plots of the stress resultants as a function of time. In all cases, the dynamic solution appears realistic and oscillates about the static value. The effect of nonlinearities was not highly significant for the loading considered.

COMPUTER PROGRAM

The analysis and numerical solution described herein have been programmed in double precision in the FORTRAN IV language and carried out on an IBM 360/65 computer. For computation efficiency, the computer code is logically separated into two parts. The first code, called DYNASOR I (DYnamic Nonlinear Analysis of Shells Of Revolution), accepts a description of the structure, generates stiffness and mass matrices, and writes them on tape for input to the second code, DYNASOR II. DYNASOR II generates generalized forces from a mechanical and thermal load history, reads the stiffness and mass matrices from tape, and then solves the initial value problem based upon given initial displacements and velocities.

Segmenting the computer code in this manner has several advantages. Once an element configuration for a structure is selected, DYNASOR I is executed only once at which time stiffness and mass matrices for up to twenty Fourier cosine harmonics are generated and stored on tape. DYNASOR II then uses this tape as input to perform analyses using various loading conditions, time increments, or harmonic numbers without having to generate stiffness and mass properties anew for each analysis. This results in the saving of a considerable amount of computer time, especially if a large number of analyses are performed on the same structure. A maximum of five harmonics is permitted in the solution by DYNASOR II with the selection of which harmonics to use being based on the particular problem at hand. The program automatically scans the tape and inputs only stiffness and mass matrices for those harmonics which are requested. In

addition, other computer codes can be interfaced with DYNASOR I so that they utilize the stiffness, mass, and other properties stored on tape. SNASOR II, a computer code presently under development for the static nonlinear analysis of shells of revolution, accepts this tape as input so that stiffness properties do not have to be generated. In addition, a program to calculate mode shapes and frequencies utilizes the mass and stiffness matrices stored on this tape.

Considerable time has been devoted to making the computer program an efficient, versatile, and easy to use code. To avoid the tedious task of inputting the coordinates and slopes at individual nodal points, several subroutines have been included in DYNASOR I which automatically generate this information with only a minimum of input data required. The program will generate the geometry for any shell of revolution the meridian of which can be made up of a combination of straight lines, circular arcs, or parabolic sections.

The mechanical load history is described by specifying the pressure distribution over the element at discrete time intervals with a linear variation being assumed between the specified times. For a particular element, the pressure distribution is assumed to be constant in the meridional direction and to vary as a step function in the circumferential direction. The thermal load history is described similarly by either inputting the temperature and temperature gradient distribution or by inputting the Fourier coefficients for the temperature and temperature gradient distribution.

The computer code has a restart provision permitting the program to be restarted at a particular time increment once the program has been run up to that time increment. The program allows restart information to be placed on tape periodically during the execution of DYNASOR II. If subsequent analysis of the output indicates that a smaller time increment is needed, then the program can be automatically cycled to any time increment for which restart information is stored on tape and then the analysis restarted with a small time increment. This restart feature can save a considerable amount of computer time particularly in buckling analyses.

The computational effort required in evaluating the nonlinear terms has been considerably lessened since the original method described in Ref. 4. Rather than evaluating these nonlinearities in terms of the α coefficients and then transforming back to the cylindrical coordinate system, the nonlinearities are written in finite difference form directly in terms of the generalized nodal coordinates. In addition, the third and fourth order trigonometric integrals discussed in Eq. 12 are evaluated exactly and stored in an array rather than calculating them each and every time they are needed. In practice, it turns out that most of these integrals are zero. Consequently, program logic is organized so that when the integrals for a particular harmonic combination are zero, the program automatically skips the calculation of the nonlinear terms since needless calculation would result only in a zero contribution. The solution of the linear algebraic set of equilibrium equations is facilitated through the use of an efficient Gaussian elimination procedure.

To minimize storage requirements, the stiffness matrix is arranged as a one-dimensional array with only the upper band portion of the symmetric stiffness matrix being stored. The solution of 204 equilibrium equations requires less than 0.1 seconds on the IBM 360/65.

The program output consists of all input control words, input loads and temperatures, generalized forces, stiffness and mass matrices, and the resultant displacements and stress resultants. The displacements and stress resultants are printed at all or any of the time increments specified and for as many circumferential angles as desired.

The program, as written for the IBM 360/65 computer, allows a solution using up to fifty elements and five Fourier harmonics. In double precision, DYNASOR I requires approximately 96,000 bytes of storage while DYNASOR II requires 282,000 bytes. Both programs require one scratch disk and one disk or tape for permanent storage of the stiffness and mass properties of the structure. Considering the complexity of the computer program, it is extremely efficient. For example, the single precision solution to the problem in Fig. 16 using thirty elements and three harmonics was obtained in 13 minutes. The double precision solution to the problem in Fig. 20 using one harmonic and fifty elements required 7 minutes. In double precision, approximately 0.4 seconds of computer time are required per time cycle using one Fourier harmonic and fifty elements. For five harmonics and fifty elements, 4 seconds are required per time cycle. Few moderately nonlinear problems will require more than thirty minutes of computer time on the IBM 360/65. With other computers, such as the CDC 6600, this time could be cut appreciably and the allowable number of harmonics and elements increased.

CONCLUSIONS

A formulation and computer code has been developed which allows the solution of problems in the nonlinear dynamic analysis of shells of revolution in reasonable periods of time on the computer. Use of the computer code has been demonstrated through the solution of a wide class of difficult and practical problems.

The particular noteworthy features of the formulation are:

1. The nonlinear terms are taken to the right-hand side of the equations of equilibrium and treated as psuedo forces.
2. The nonlinear terms are evaluated by using linear displacements in the meridional distance, s , for the normal displacement, w , as well as the meridional and circumferential displacements. Rapid convergence of results with mesh refinement is observed.
3. Houbolt's method of solution is extended to treat nonlinear problems by using a linear extrapolation to obtain the nonlinear psuedo loads at $t + \Delta t$ in terms the loads at t and $t - \Delta t$. It is demonstrated that this procedure is stable for highly nonlinear problems.

The method of solution which proved to be the most stable is Houbolt's method with the nonlinear terms being determined by a first order Taylor's expansion. Undoubtedly, the use of a Taylor's expansion contributes to making the method unstable for large time increments; but, in spite of this, Houbolt's method is more stable than the other numerical methods which do not require an extrapolation of the loads.

REFERENCES

1. Turner, M. J., Dill, E. H., Martin, H. C., and Melosh, R. J., "Large Deflections of Structures Subjected to Heating and External Loads," *J. Aerospace Science*, Vol. 27, No. 2, Feb. 1960, pp. 97-107.
2. Martin, H. C., "Finite Element Formulation of Geometrically Nonlinear Problems," *Proceedings Japan-U.S. Seminar on Matrix Methods in Structural Analysis and Design*, Tokyo, Japan, 1969.
3. Oden, J. T., "Finite Element Applications in Nonlinear Structural Analysis," *Proceedings, Conference on Finite Element Methods*, Vanderbilt University, Nashville, Tennessee, November, 1969.
4. Stricklin, J. A., Haisler, W. E., MacDougall, H. R., and Stebbins, F. J., "Nonlinear Analysis of Shells of Revolution by the Matrix Displacement Method," *AIAA Journal*, Vol. 6, No. 12, Dec. 1968, pp. 2306-2312.
5. Witmer, E. A., Balmer, H. A., Leech, J. W., and Pian, T. H. H., "Large Dynamic Deformations of Beams, Rings, Plates, and Shells," *AIAA Journal*, Vol. 1, No. 8, August 1963, pp. 1848-1857.
6. Krieg, R. D. and Duffey, T. A., "Univalve II - A Code to Calculate the Large Deflection Dynamic Response of Beams, Rings, Plates and Cylinders," Sandia Laboratories, Albuquerque, New Mexico, Report SC-RR-68-303, October 1968.
7. Duffey, T. A. and Key, S. W., "Experimental-Theoretical Correlations of Impulsively Loaded Clamped Circular Plates," Sandia Laboratories, Albuquerque, New Mexico, Report SC-RR-69-1225, June 1969.
8. Krieg, R. D., Duffey, T. A., and Key, S. W., "The Large Deflection Elastic-Plastic Response of Impulsively Loaded Beams: A Comparison Between Computations and Experiment," Sandia Laboratories, Albuquerque, New Mexico, Report SC-RR-68-226, July 1968.
9. Balmer, H. A. and Witmer, E. A., "Theoretical-Experimental Correlation of Large Dynamic and Permanent Deformations of Impulsively Loaded Simple Structures," Massachusetts Institute of Technology, Aeroelastic and Structures Research Laboratory, FDL-TDR-64-108, July 1964.
10. Leech, J. W., Witmer, E. A., and Pian, T. H. H., "Numerical Calculation Technique for Large Elastic-Plastic Transient Deformation of Thin Shells," *AIAA Journal*, Vol. 6, No. 12, Dec. 1968, pp. 2352-2359.
11. Wrenn, B. G., Sobel, L. H., and Silsby, W., "Nonsymmetric and Nonlinear Response of Thin Shells," Lockheed Missiles and Space Co., Palo Alto, California, Report LMSC B-72-67-3, Dec. 1967.
12. Leech, J. W., Hsu, P. T., and Mack, E. W., "Stability of a Finite Difference Method for Solving Matrix Equations," *AIAA Journal*, Vol. 3, No. 11, Nov. 1965, pp. 2172-2173.

13. Johnson, D. E., "A Proof of the Stability of the Houbolt Method," AIAA Journal, Vol. 4, No. 8, Aug. 1966, pp. 1450-1451.
14. Krieg, R. D., "Numerical Stability of a Finite Differencing of the Nonlinear Underwater Taut String Problem," SC-TM-69-265, Sandia Laboratories, Albuquerque, New Mexico 1969.
15. Nickell, R. E., "On the Stability of Approximation Operators in Problems of Structural Dynamics," MM 69-4116-14, Bell Telephone Laboratories, Whippny, New Jersey, 1969.
16. Stricklin, J. A., Navaratna, D. R., and Pian, T. H. H., "Improvements on the Analysis of Shells of Revolution by the Matrix Displacement Method," AIAA Journal, Vol. 4, No. 11, Nov. 1966, pp. 2069-2072.
17. Grafton, P. E. and Strome, D. R., "Analysis of Axisymmetric Shells by the Direct Stiffness Method," AIAA Journal, Vol. 1, No. 10, October 1963, pp. 2343-2347.
18. Novozhilov, V. V., Foundations of the Nonlinear Theory of Elasticity, Graylock Press, Rochester, N.Y., 1956.
19. Klein, S. and Sylvester, R. J., "The Linear Elastic Dynamic Analysis of Shells of Revolution by the Matrix Displacement Method," Air Force Flight Dynamics Laboratory TR-66-80, 1966, pp. 299-329.
20. Chan, S. P., Cox, H. L., and Benfield, W. A., "Transient Analysis of Forced Vibrations of Complex Structural-Mechanical Systems," Journal of Royal Aeronautical Society, Vol. 66, July 1962, pp. 475-460.
21. Stricklin, J. A. and Martinez, J. E., "Dynamic Buckling of Clamped Spherical Caps Under Step Pressure Loadings," AIAA Journal, Vol. 7, No. 6, June 1969, pp. 1212-1213.
22. Houbolt, J. C., "A Recurrence Matrix Solution for the Dynamic Response of Elastic Aircraft," Journal Aeronautical Science, Vol. 17, 1950, pp. 540-550.
23. Bushnell, D. "Nonlinear Analysis for Axisymmetric Elastic Stresses in Ring-Stiffened Segmented Shells of Revolution," paper presented at AIAA/ASME 10th Structures, Structural Dynamics and Materials Conference, New Orleans, Louisiana, April 1969.
24. Zienkiewicz, O. C. and Cheung, Y. K., The Finite Element Method in Structural and Continuum Mechanics, McGraw-Hill, 1966, pp. 24-25.
25. Tillerson, J. R., "Numerical Methods of Integration Applied in the Nonlinear Dynamic Analysis of Shells of Revolution," to be submitted to satisfy the thesis requirement for a Master of Science degree at Texas A&M University, 1970.

26. Levy, S. and Kroll, W. D., "Errors Introduced by Finite Space and Time Increments in Dynamic Response Computation," Proceedings, First U.S. National Congress of Applied Mechanics, June 1951, pp. 1-8.
27. Johnson, D. E. and Greif, R., "Dynamic Response of a Cylindrical Shell: Two Numerical Methods," AIAA Journal, Vol. 4, No. 3, March 1966, pp. 486-494.
28. Newmark, N. M. "A Method of Computation for Structural Dynamics," Proceedings of ASCE 85, EM3, pp. 67-94, 1959.
29. Hildebrand, F. B., Introduction to Numerical Analysis, McGraw-Hill Book Co., New York, 1956, p. 238.
30. Mescall, J. F., "Large Deflections of Spherical Shells Under Concentrated Loads," J. Applied Mechanics, Vol. 32, 1965, pp. 936-938.
31. Bushnell, D., "Bifurcation Phenomena in Spherical Shells Under Concentrated and Ring Loads," AIAA Journal, Vol. 5, No. 11, Nov. 1967, pp. 2034-2040.
32. Simitses, G. J., "Axisymmetric Dynamic Snap-through Buckling of Shallow Spherical Caps," AIAA Journal, Vol. 5, No. 5, May 1967, pp. 1019-1020.
33. Huang, N. C., "Axisymmetric Dynamic Snap-through of Elastic Clamped Shallow Spherical Shells," AIAA Journal, Vol. 7, No. 2, February 1969, pp. 215-220.
34. Stephen, W. B. and Fulton, R. E., "Axisymmetric Static and Dynamic Buckling of Spherical Caps due to Centrally Distributed Pressures," Paper 69-89, 1969 AIAA.
35. Lock, M. H., Okrebo, S., and Whittier, J. S., "Experiment of the Snapping of a Shallow Dome Under a Step Pressure Loading," AIAA Journal, Vol. 6, No. 7, July 1968, pp. 1320-1326.

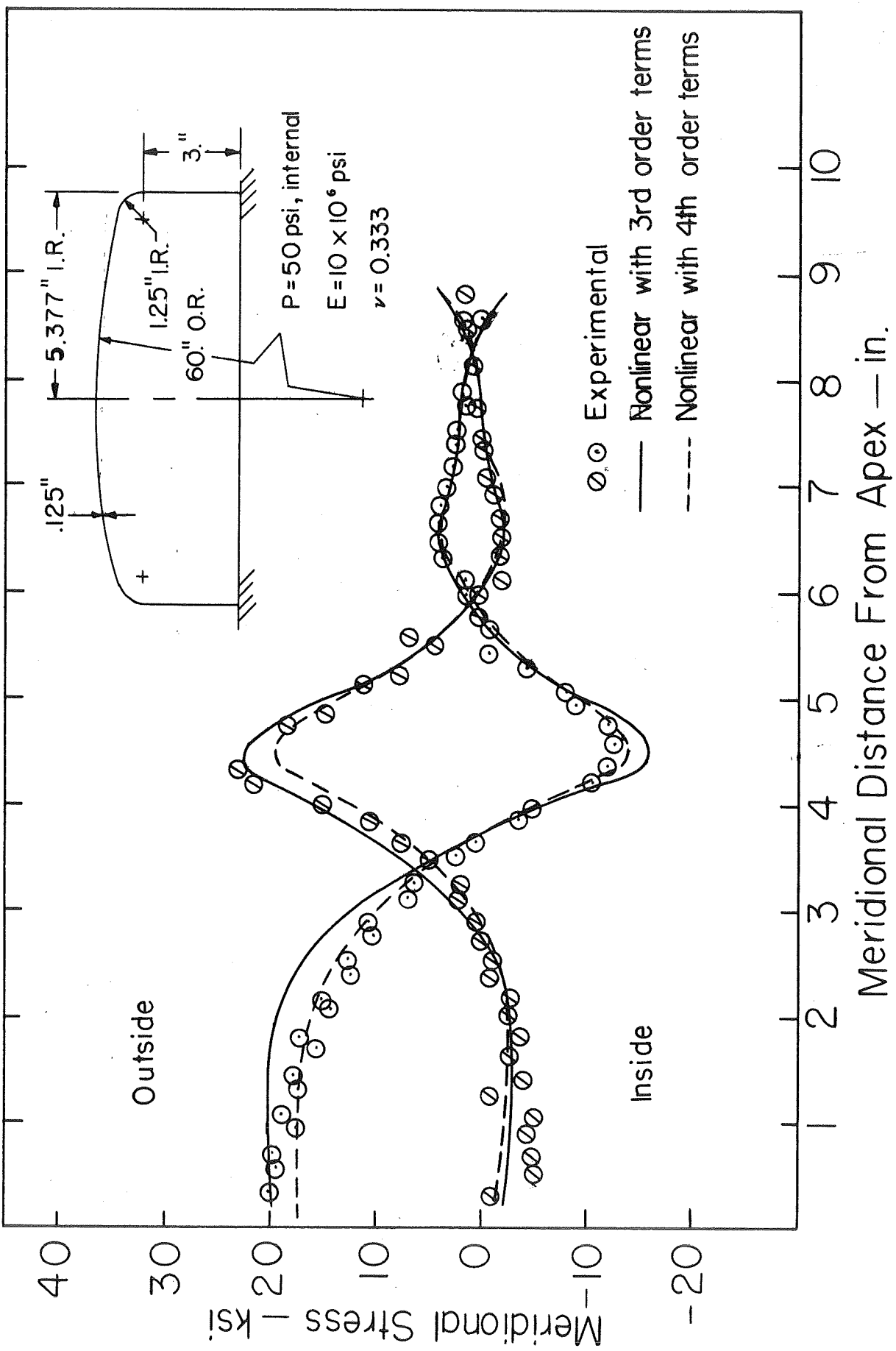


Fig. 1 MERIDIONAL STRESS ALONG ARC LENGTH

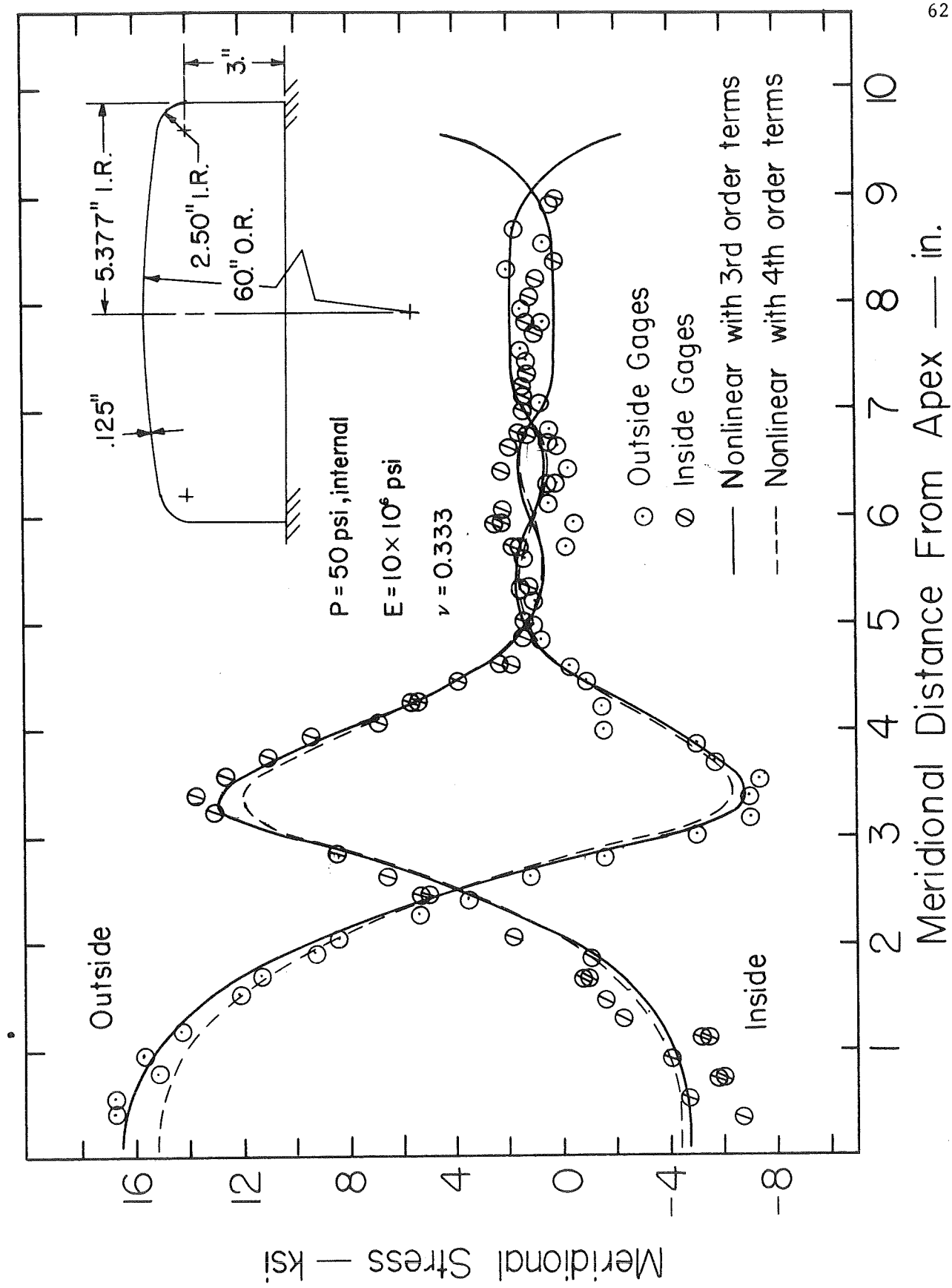


FIG. 2 MERIDIONAL STRESS ALONG ARC LENGTH

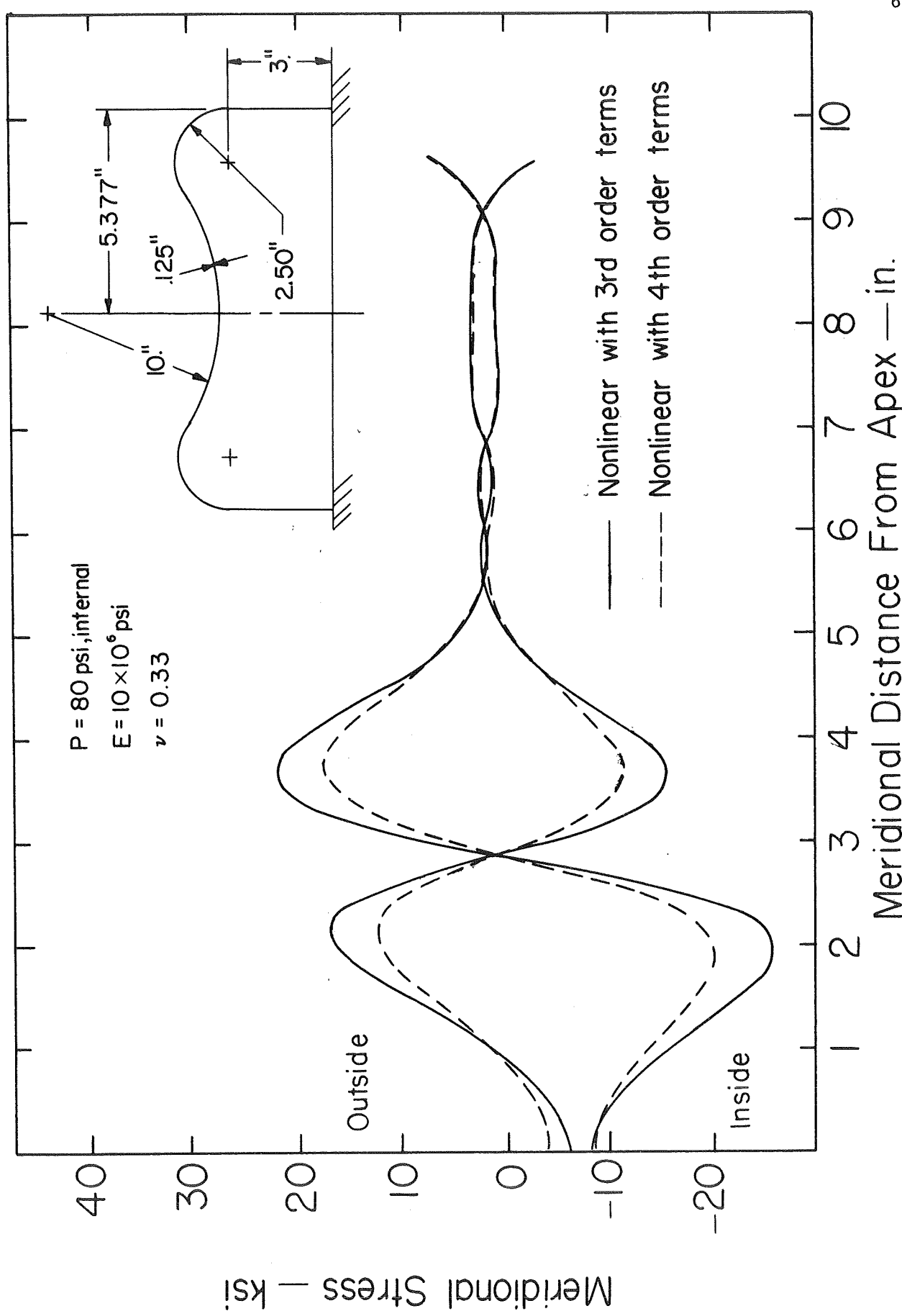


Fig. 3 MERIDIONAL STRESS ALONG ARC LENGTH

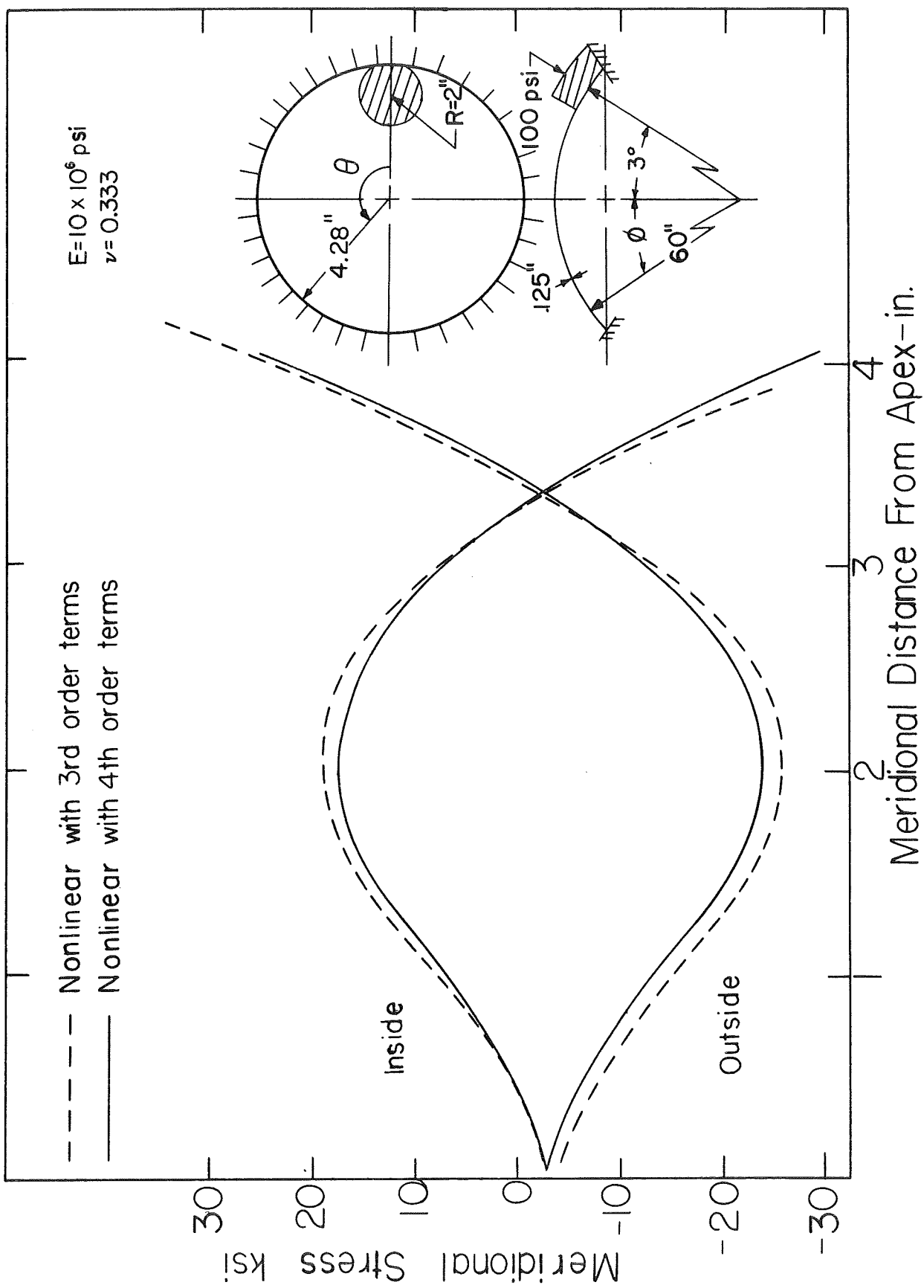


Fig. 4 MERIDIONAL STRESS ALONG ARC LENGTH

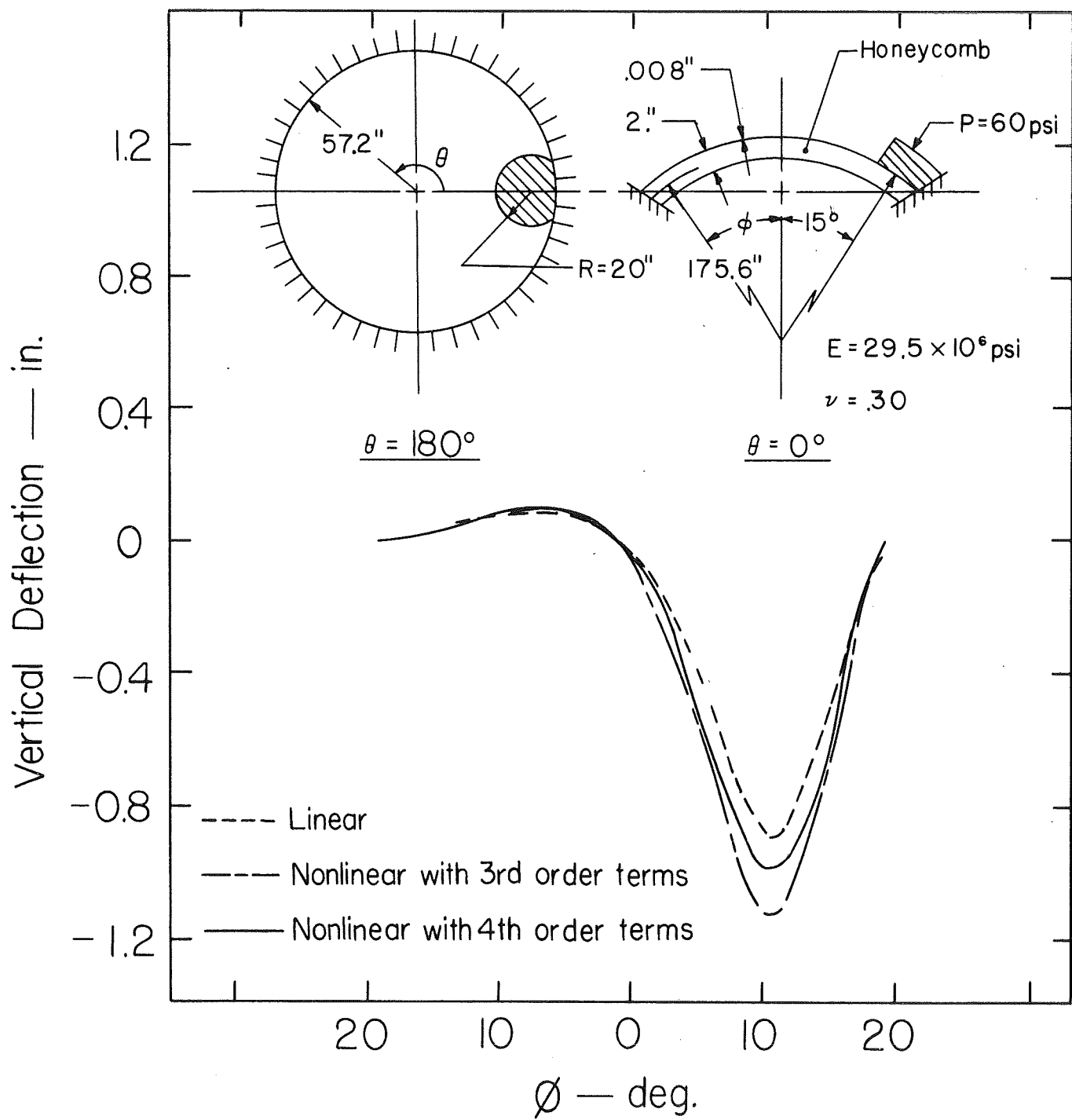


Fig. 5 DEFLECTION ALONG AXIS OF SYMMETRY

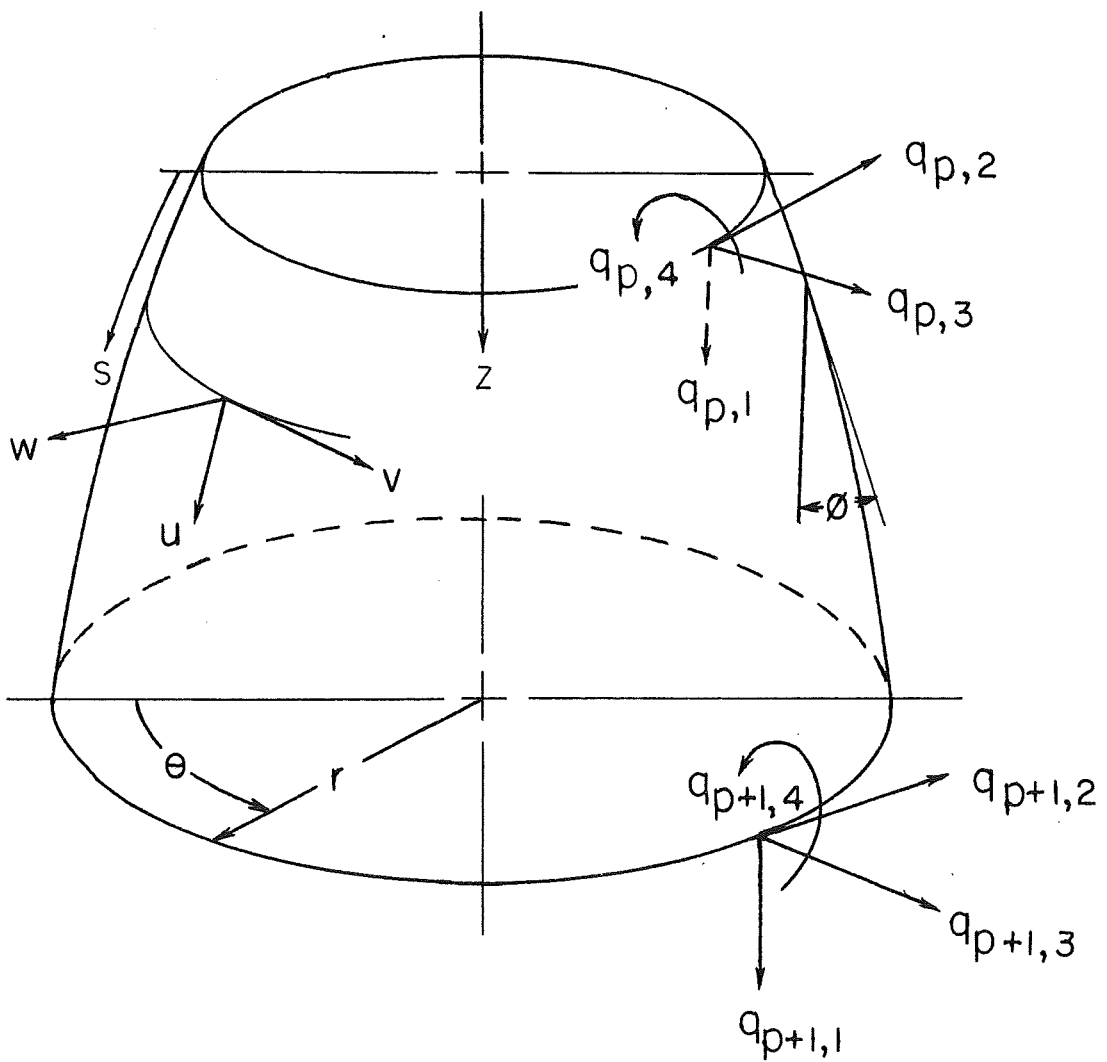


Fig. 6 GENERALIZED COORDINATES
OF SHELL ELEMENT

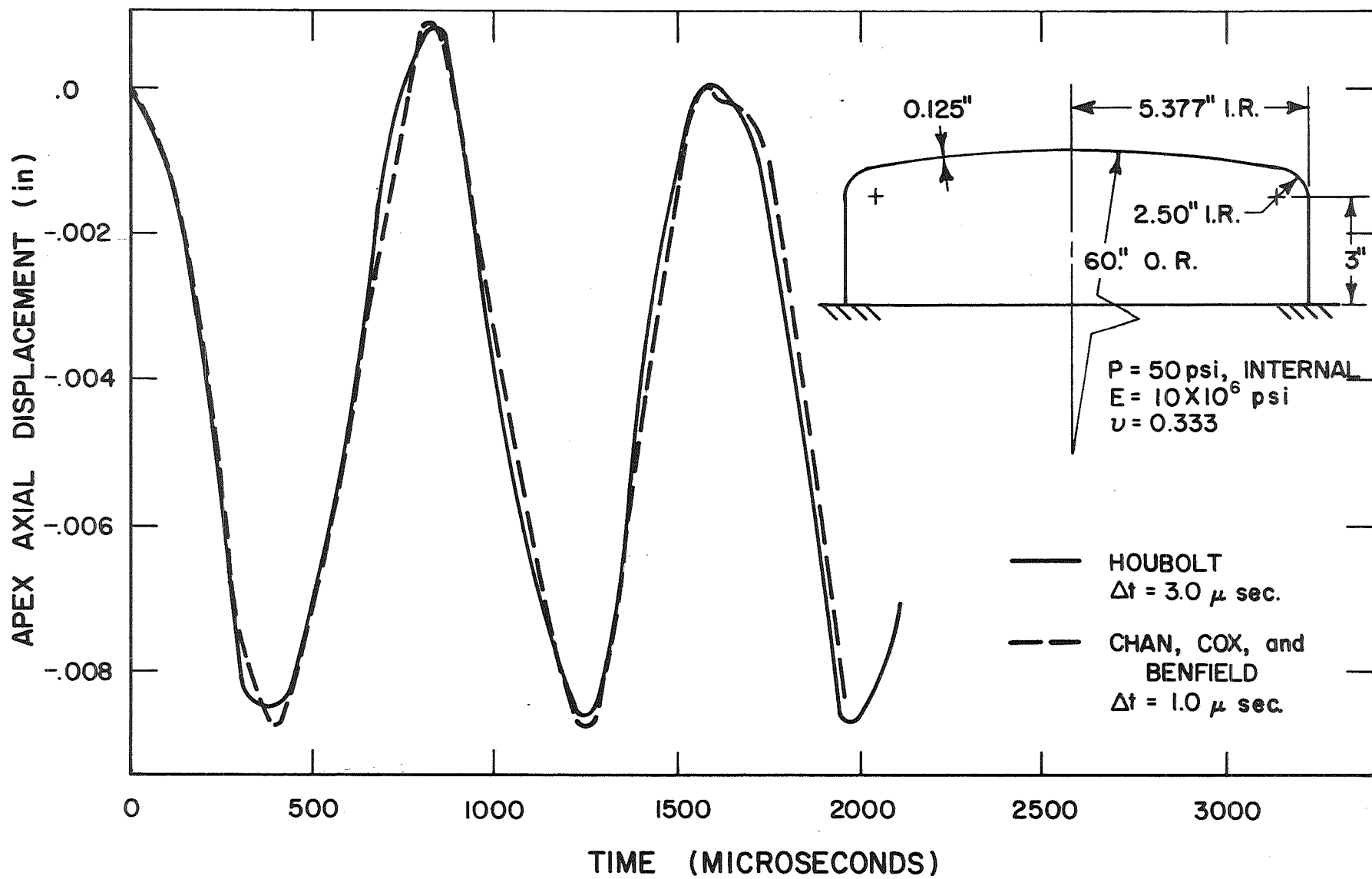


FIG. 7 DISPLACEMENT RESPONSE CALCULATED BY TWO NUMERICAL METHODS

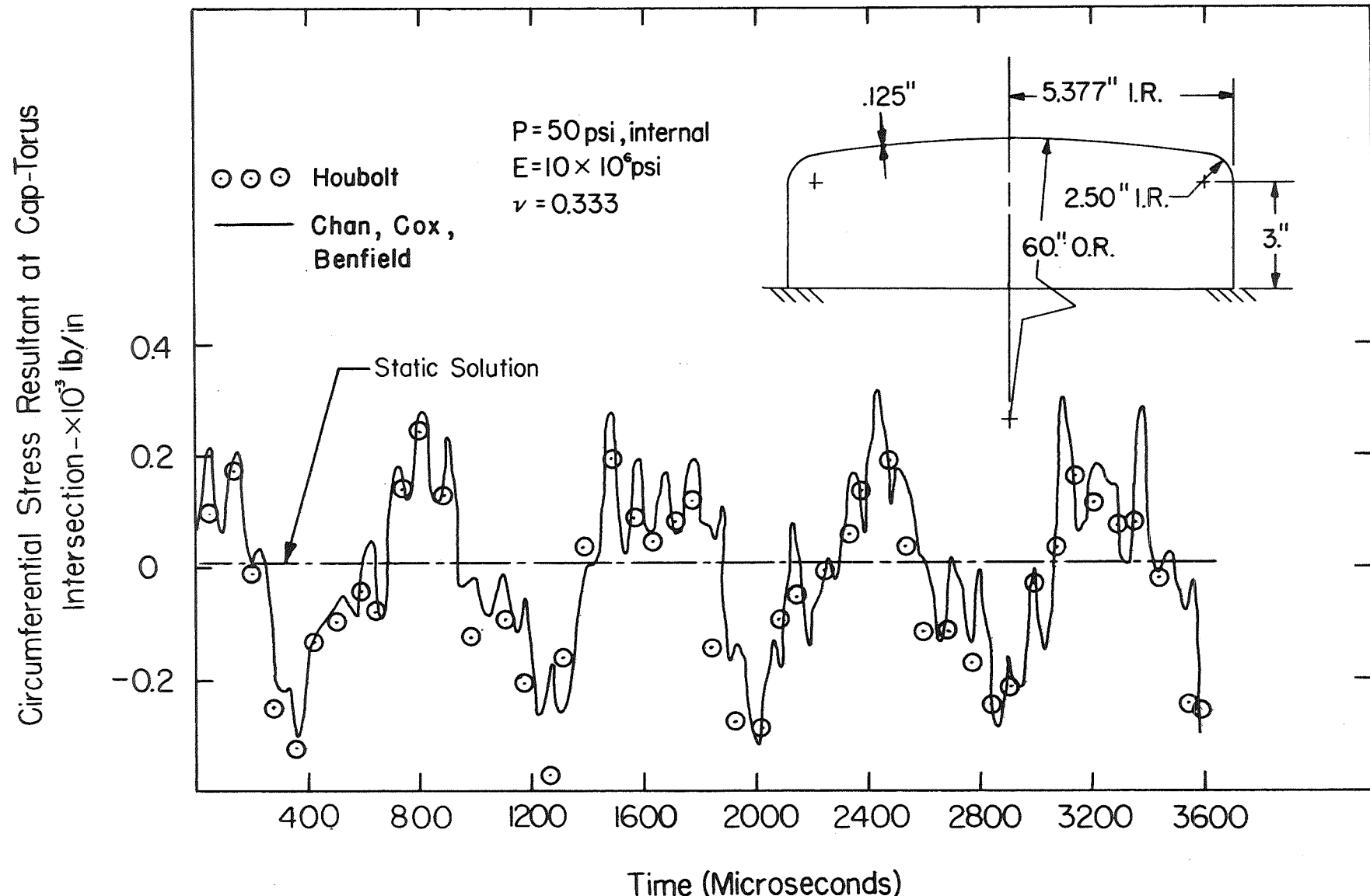


FIG. 8 CIRCUMFERENTIAL STRESS RESULTANT FOR SHELL UNDER STEP PRESSURE LOADING

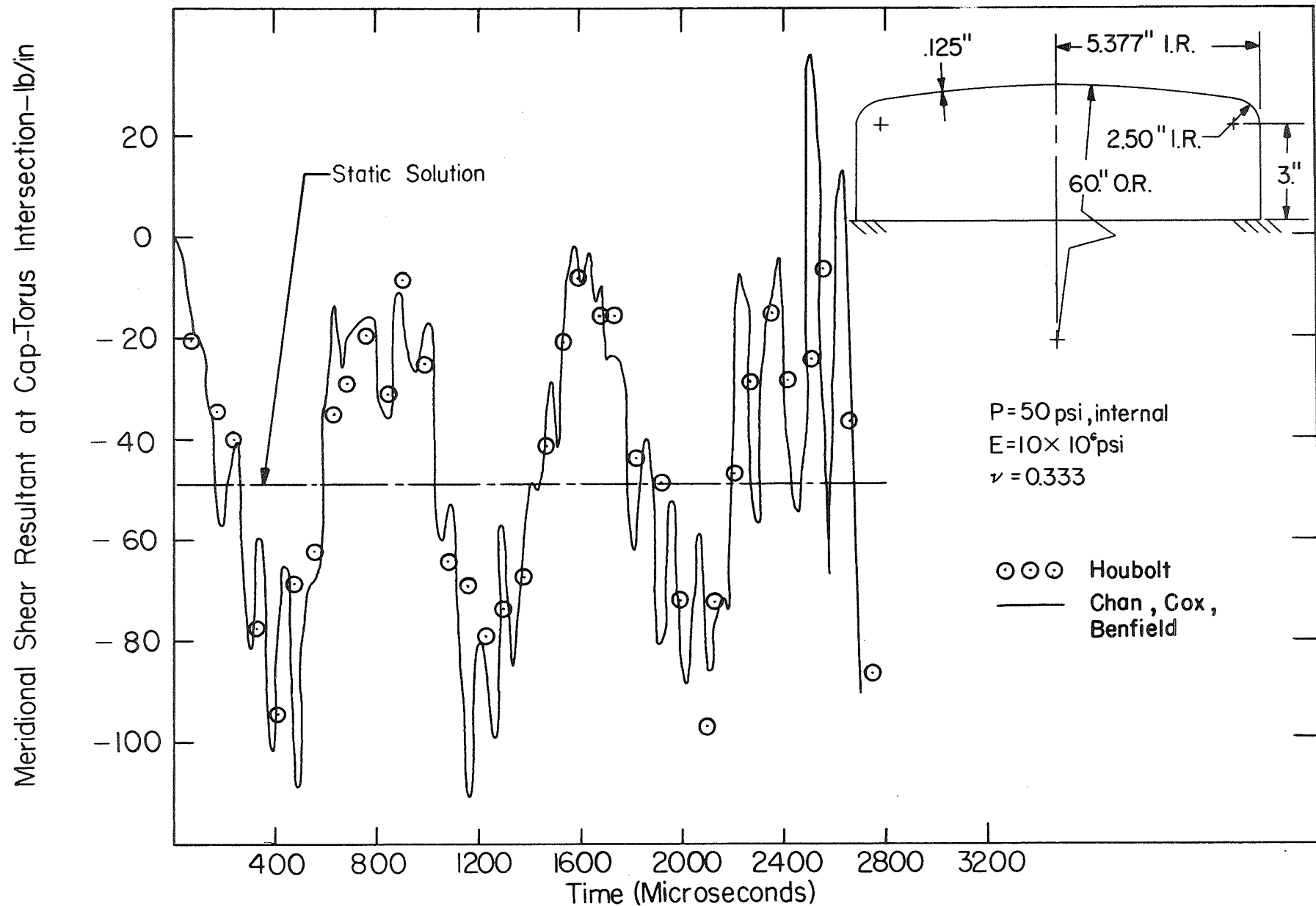


FIG. 9 MERIDIONAL SHEAR RESULTANT FOR SHELL UNDER STEP PRESSURE LOADING

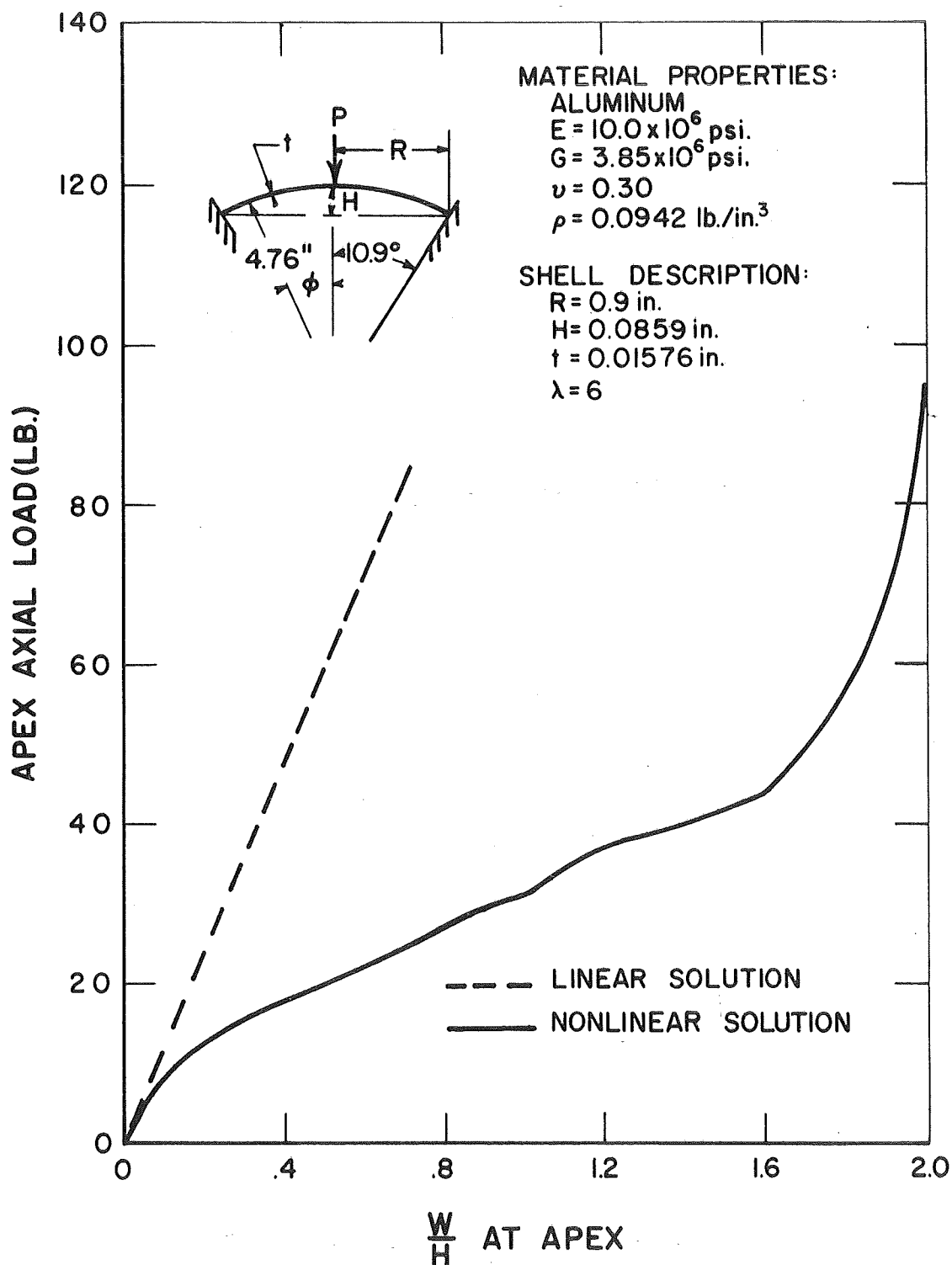


FIG. 10 STATIC RESPONSE OF SHALLOW SPHERICAL CAP

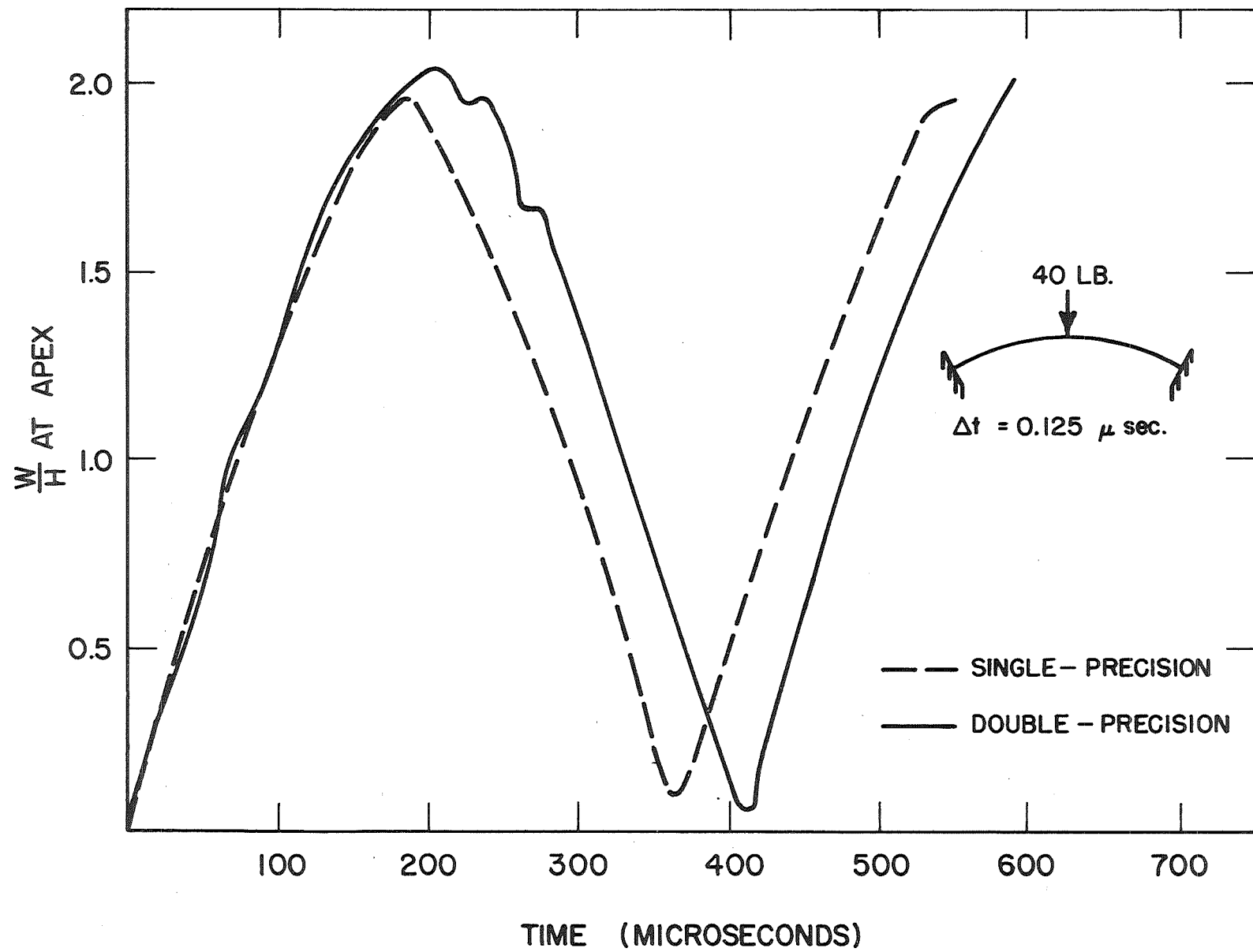


FIG. II EFFECT OF NUMERICAL ACCURACY UPON SHELL RESPONSE AT APEX

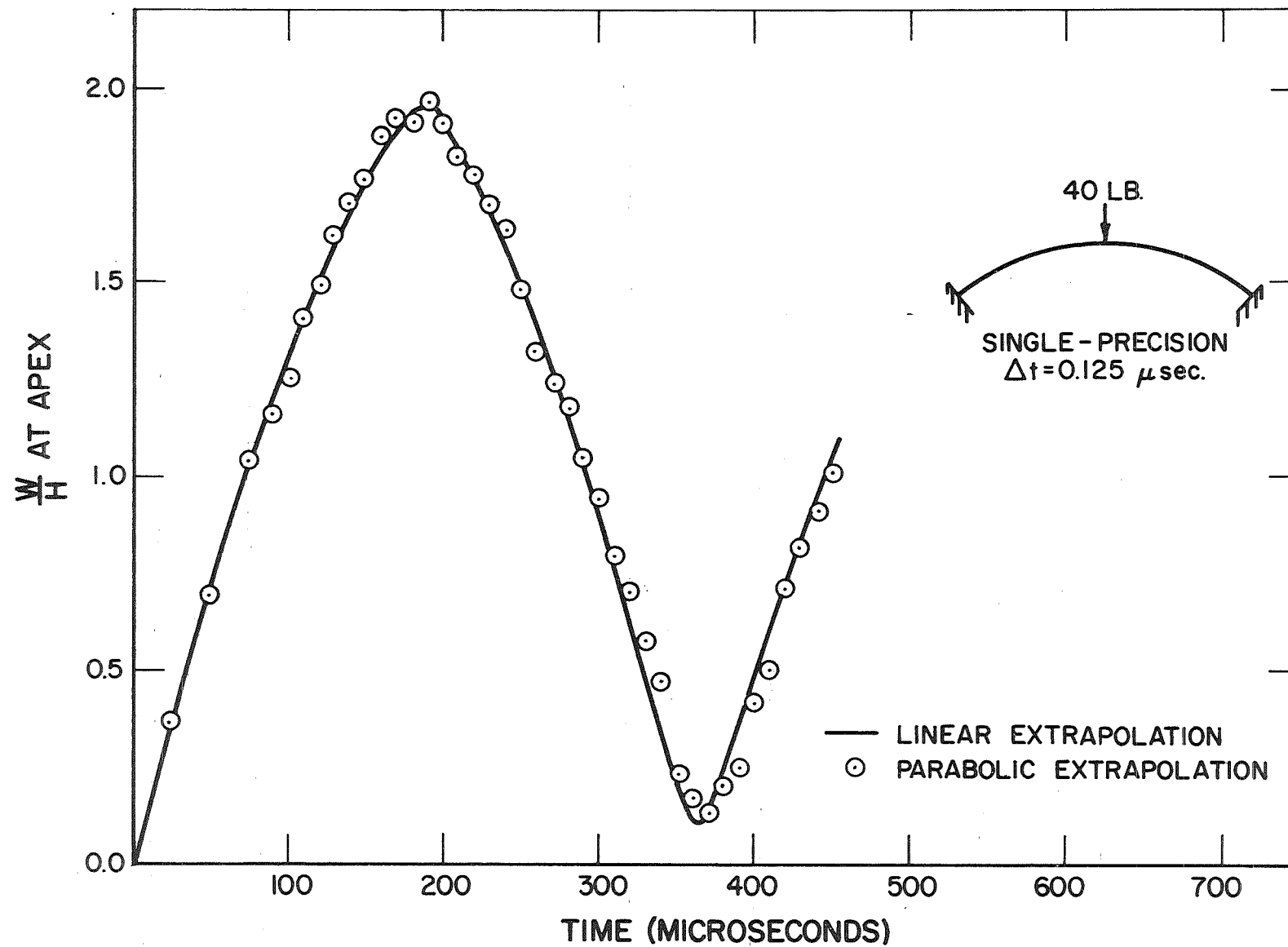


FIG. 12 EFFECT OF LOAD EXTRAPOLATION PROCEDURE UPON APEX AXIAL DISPLACEMENT

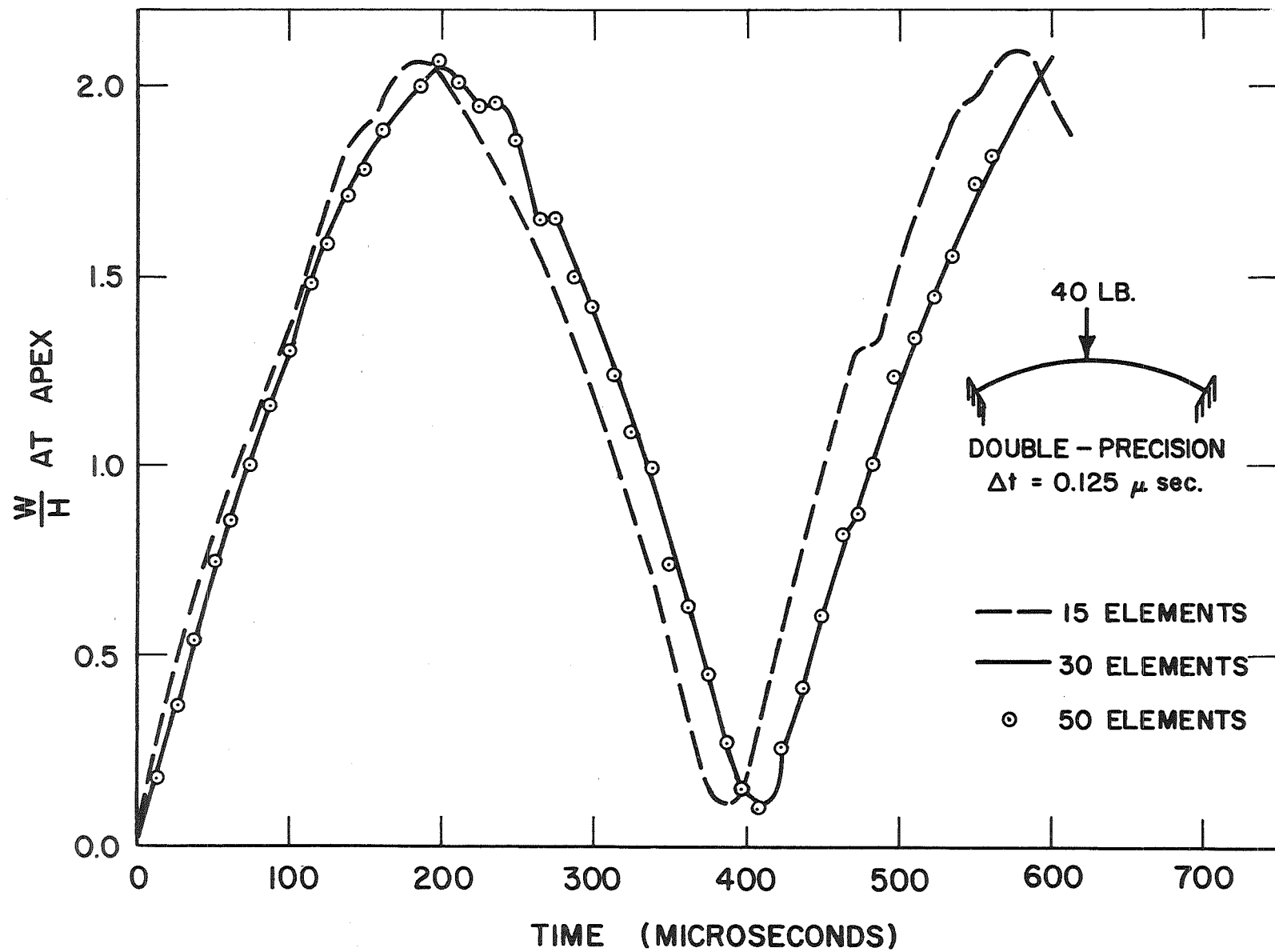


FIG. 13 SOLUTION CONVERGENCE WITH FINITE ELEMENT IDEALIZATION

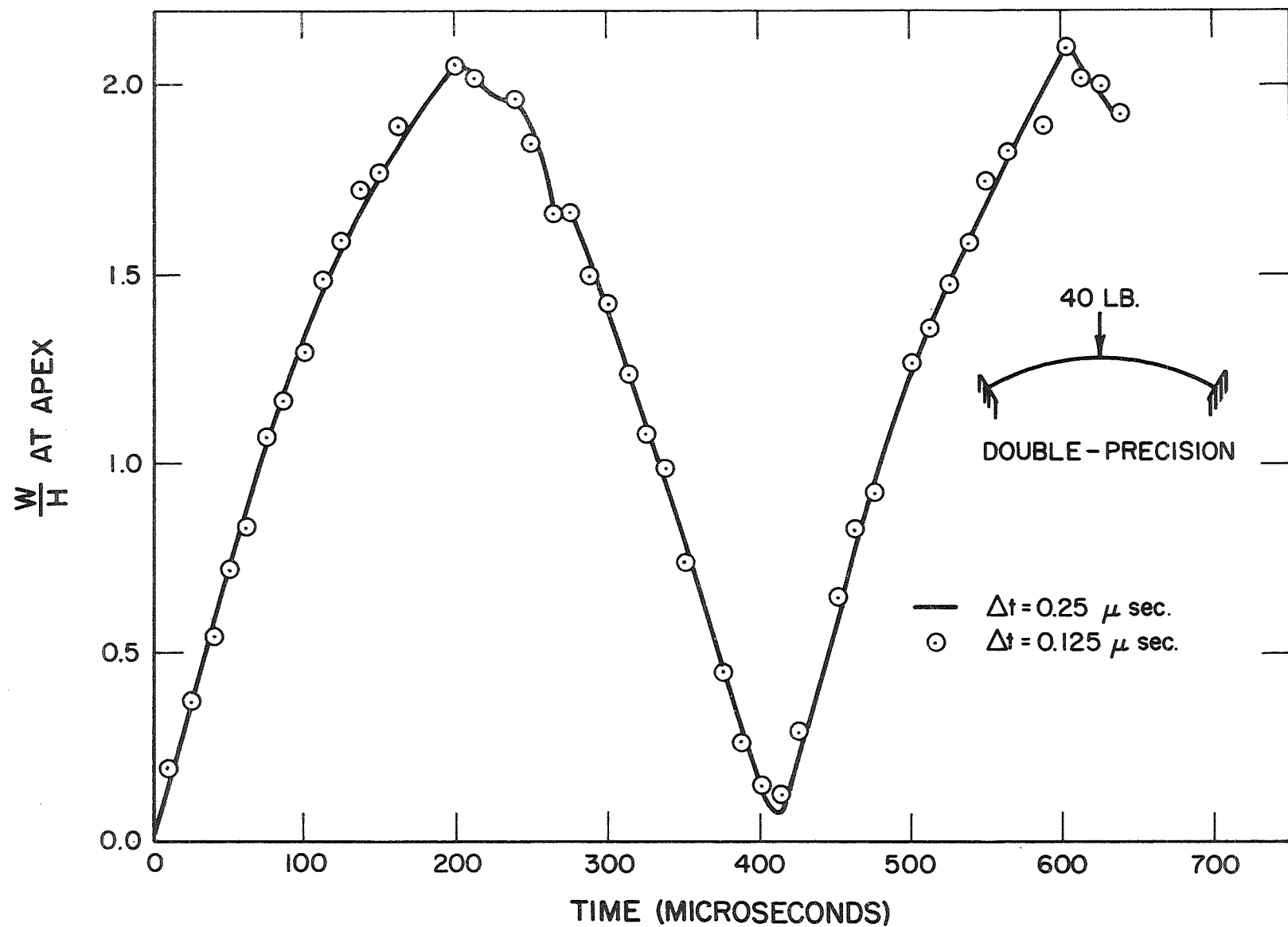


FIG. 14 EFFECT OF TIME INCREMENT UPON
APEX AXIAL DISPLACEMENT

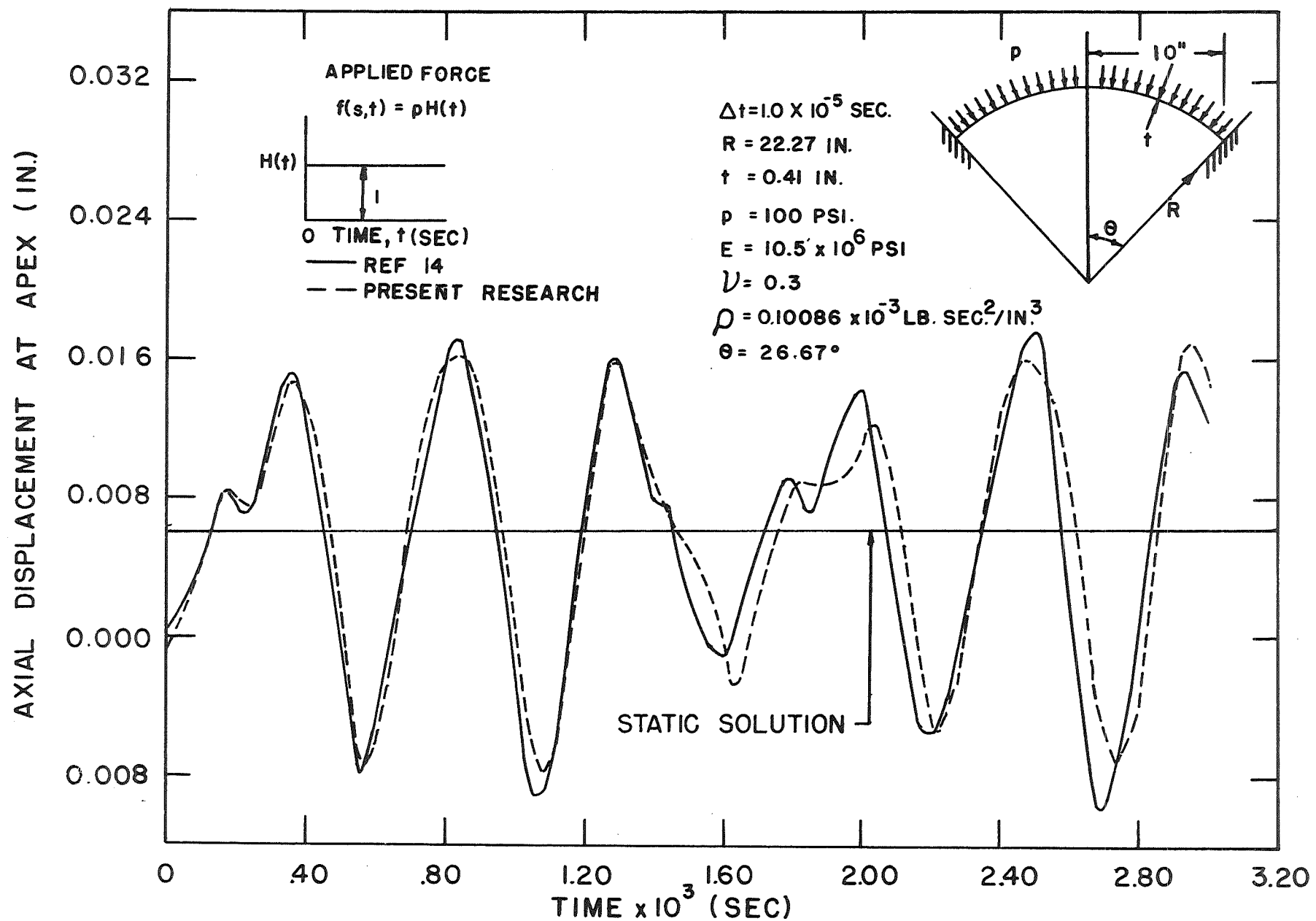


FIG. 15 SHALLOW SPHERICAL CAP UNDER AXISYMMETRIC DYNAMIC LOADING

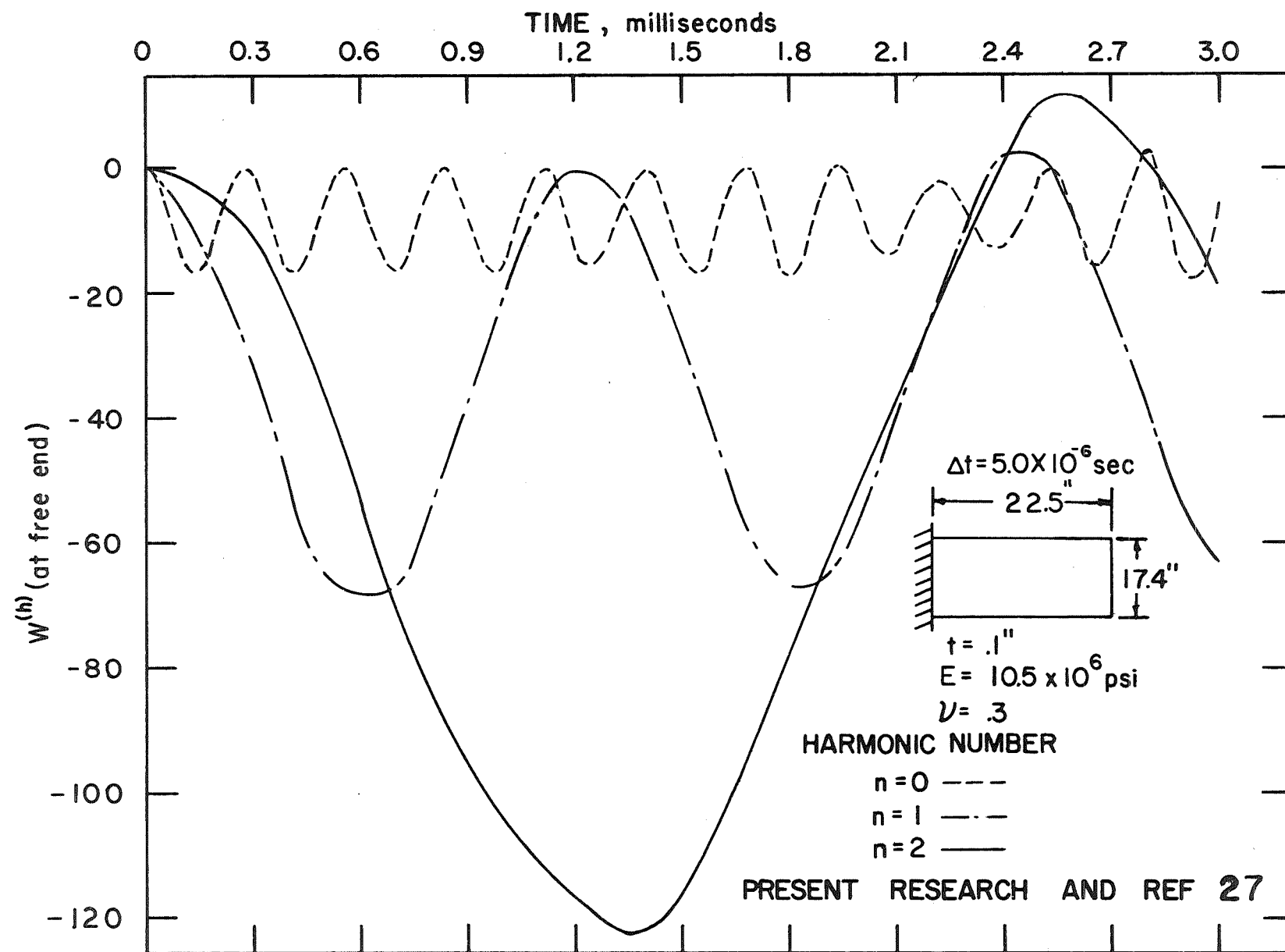


FIG. 16 NONDIMENSIONAL FOURIER COEFFICIENT OF NORMAL DISPLACEMENT
VERSUS TIME FOR CYLINDER UNDER ASYMMETRICAL LOADING

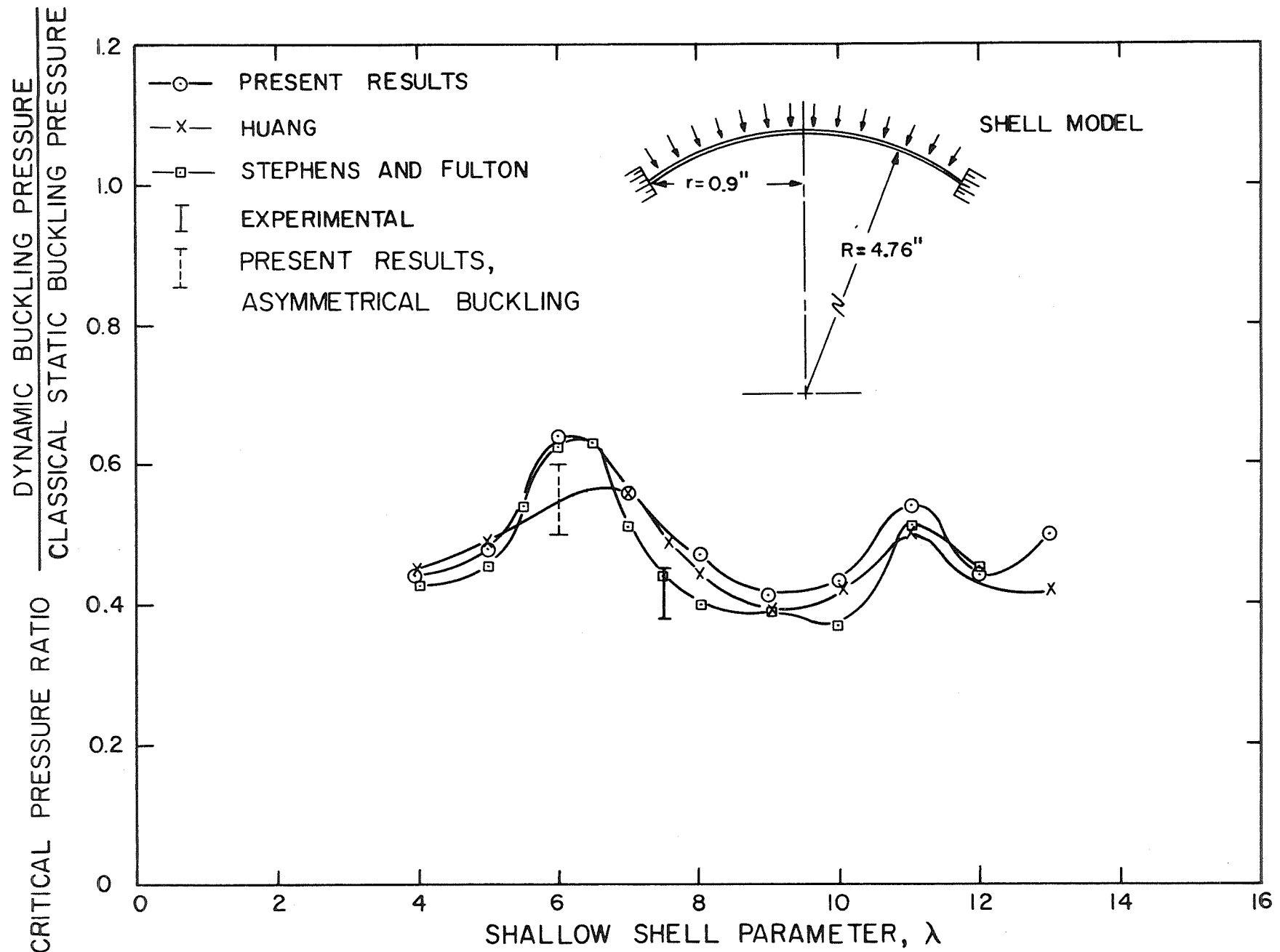


FIG. 17 CRITICAL PRESSURE RATIO AS A FUNCTION OF THE SHALLOW SHELL PARAMETER

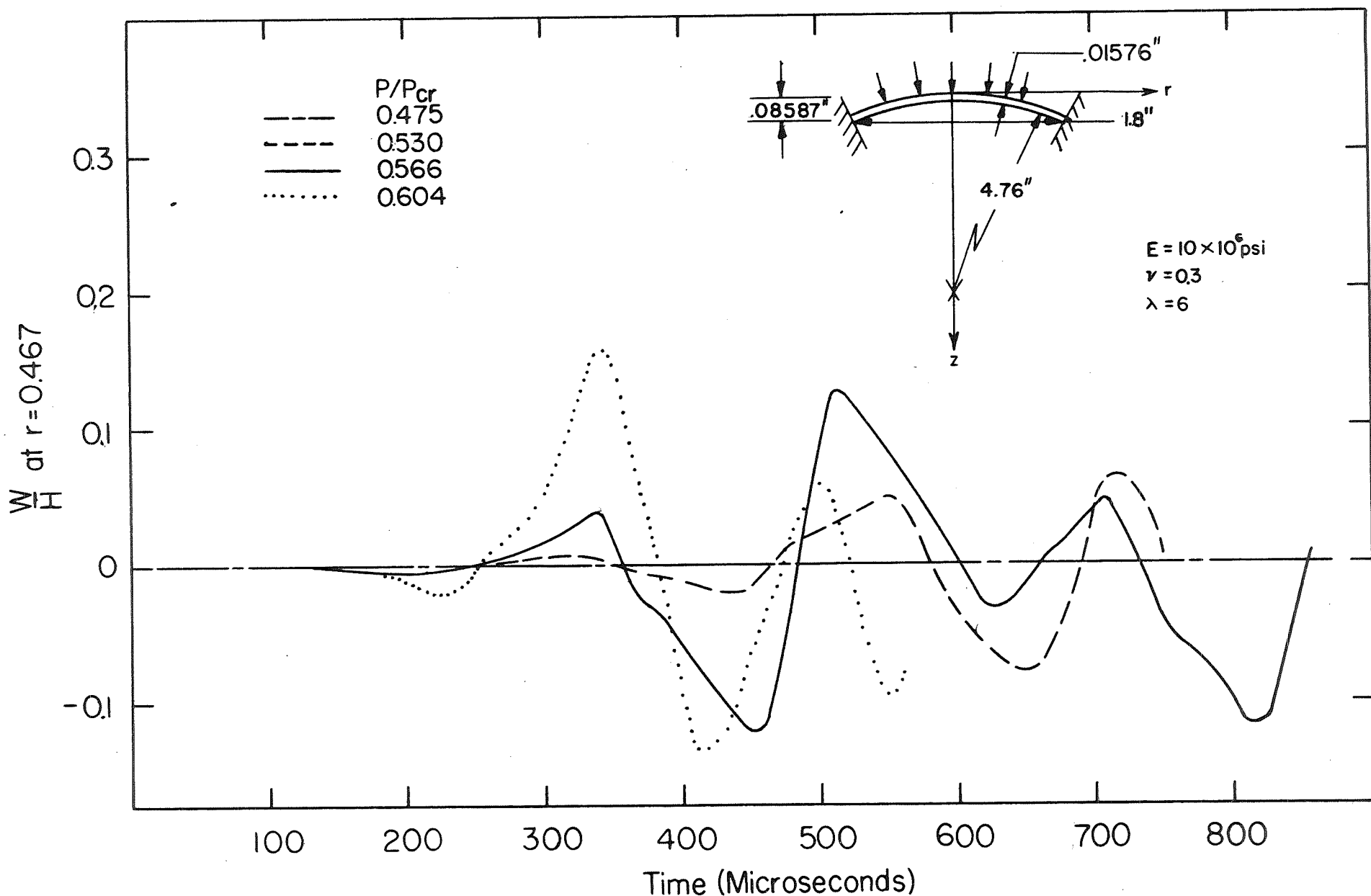


FIG. 18 RESPONSE OF 2nd HARMONIC FOR VARIOUS PRESSURE RATIOS

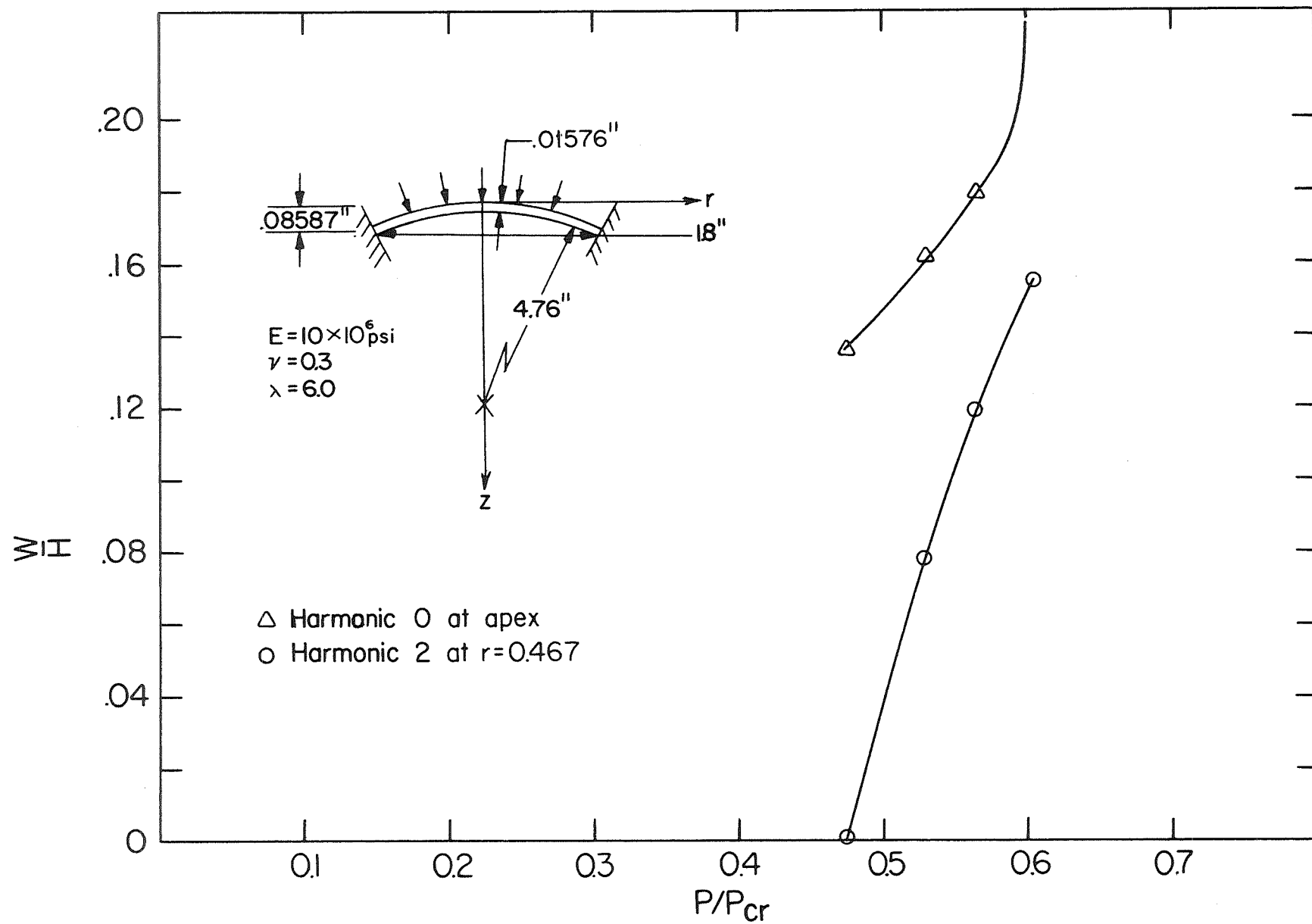


FIG. 19 PEAK RESPONSE OF HARMONIC 0 AND 2
FOR DIFFERENT PRESSURE RATIOS

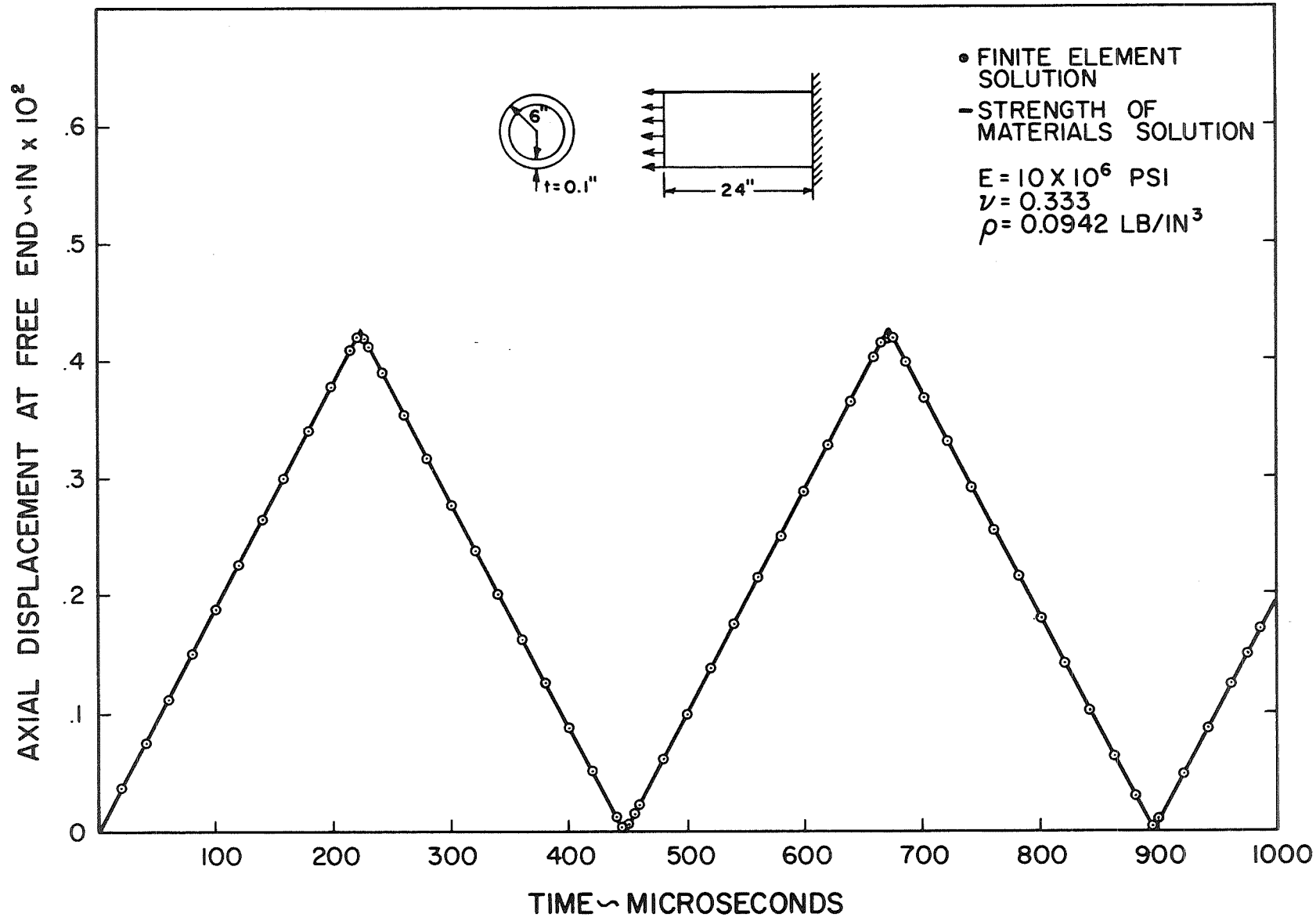


FIG. 20 DISPLACEMENT RESPONSE FOR A CYLINDER
 SUBJECTED TO SUDDENLY APPLIED AXIAL LOAD

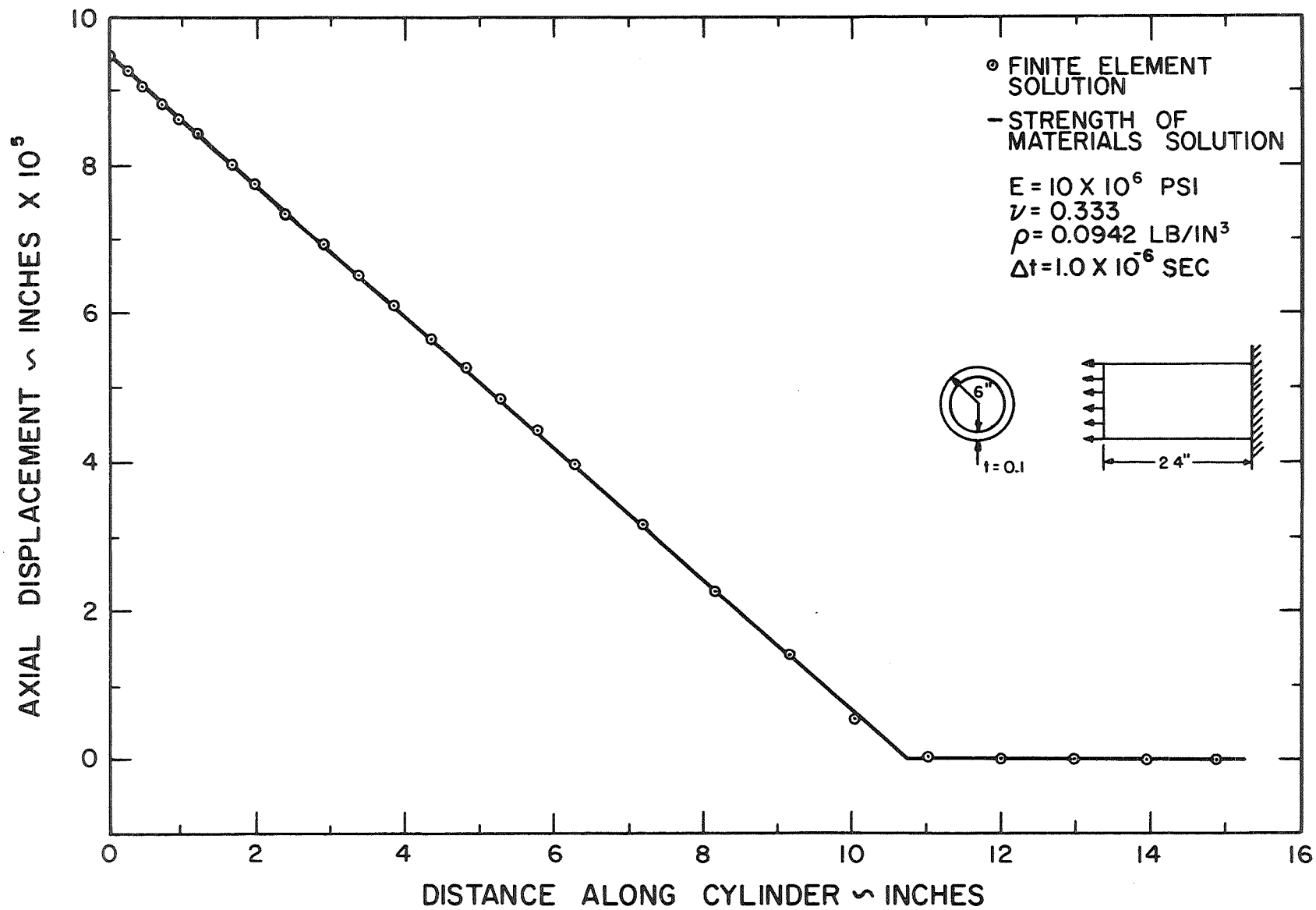


FIG. 2I AXIAL DISPLACEMENT ALONG CYLINDER
AT 50.0 MICROSECONDS

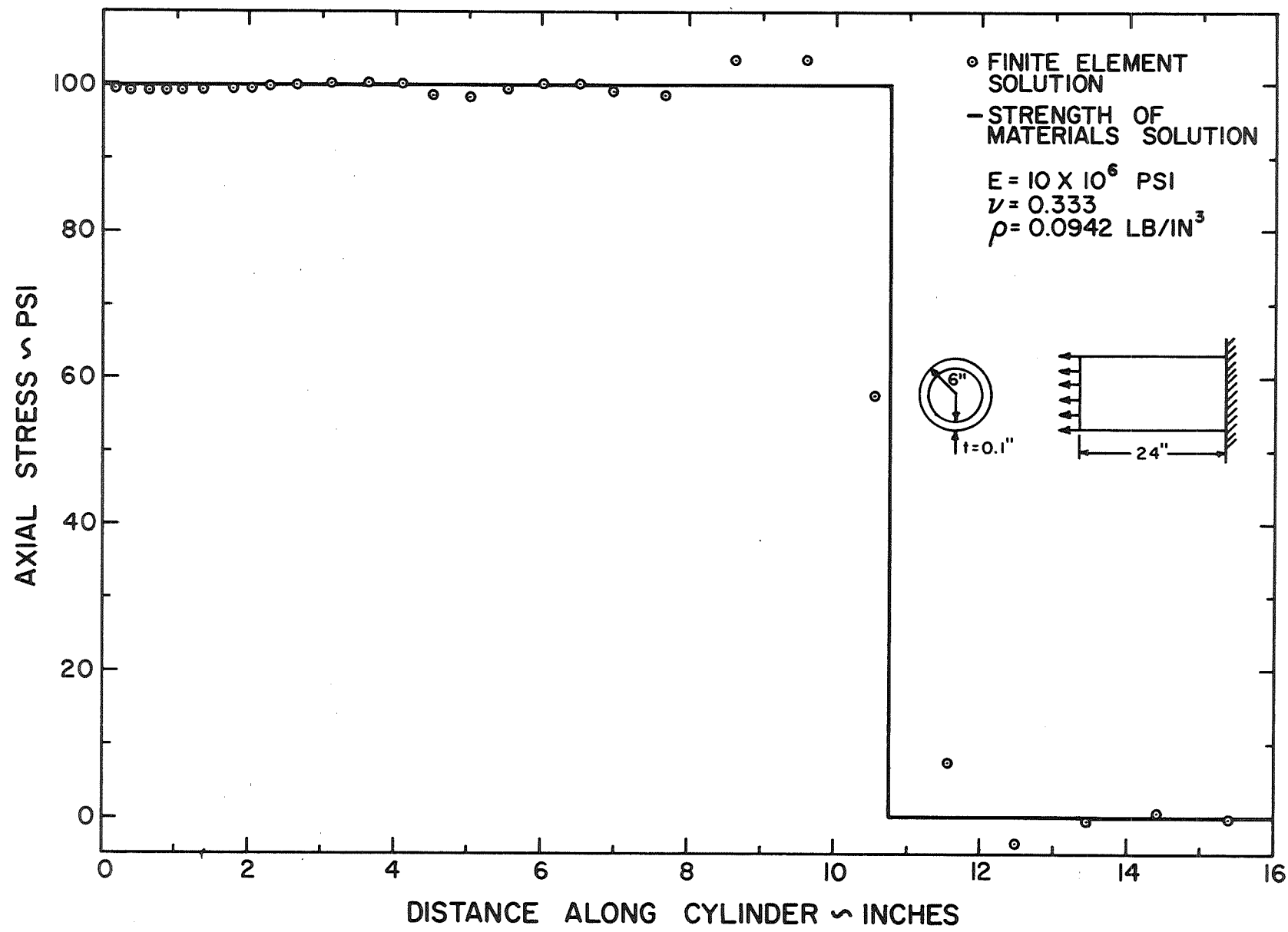


FIG. 22 AXIAL STRESS DISTRIBUTION ALONG CYLINDER
AT 50.0 MICROSECONDS

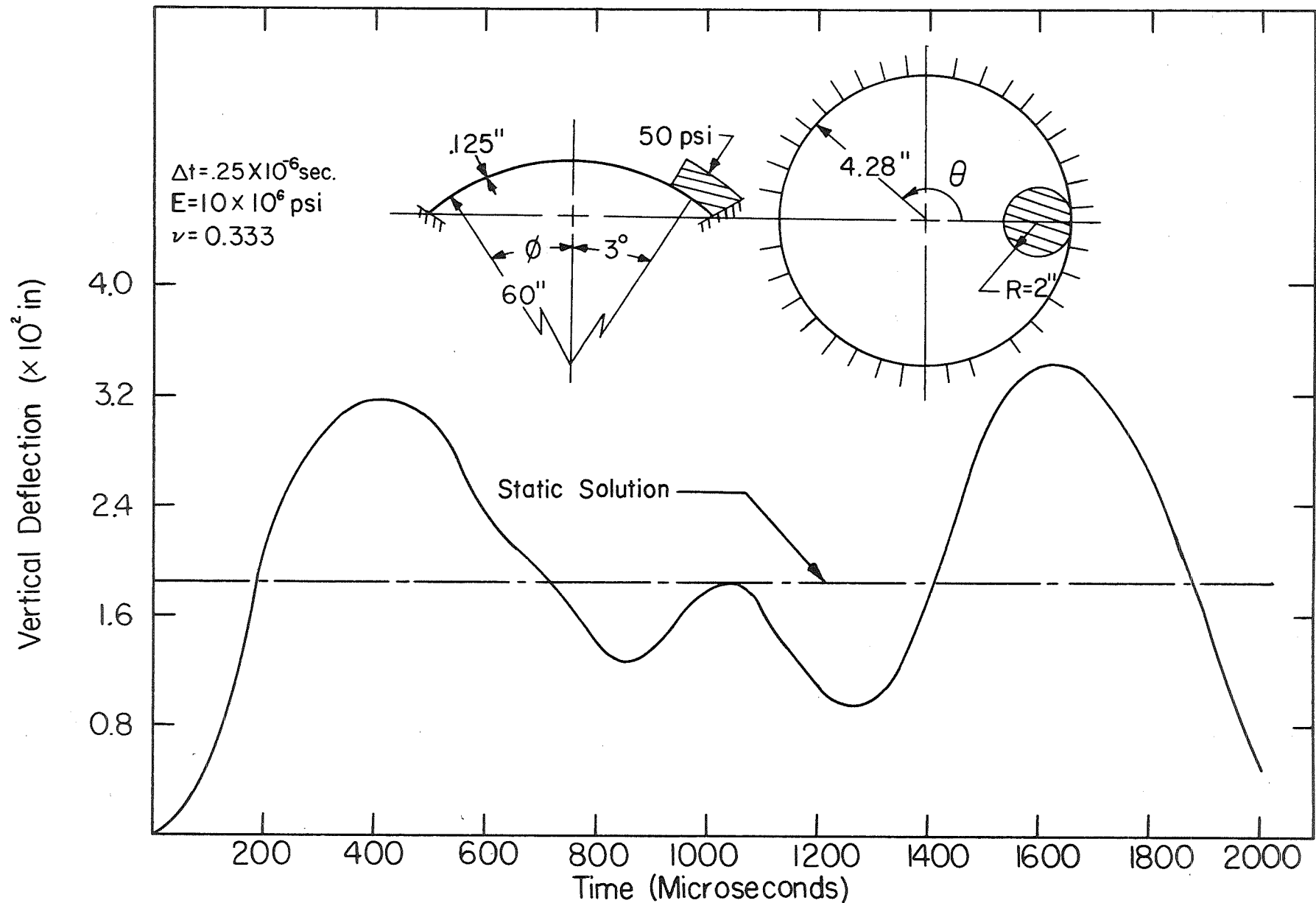


FIG. 23 VERTICAL DEFLECTION FOR SPHERICAL CAP UNDER
LOCALIZED LOADING

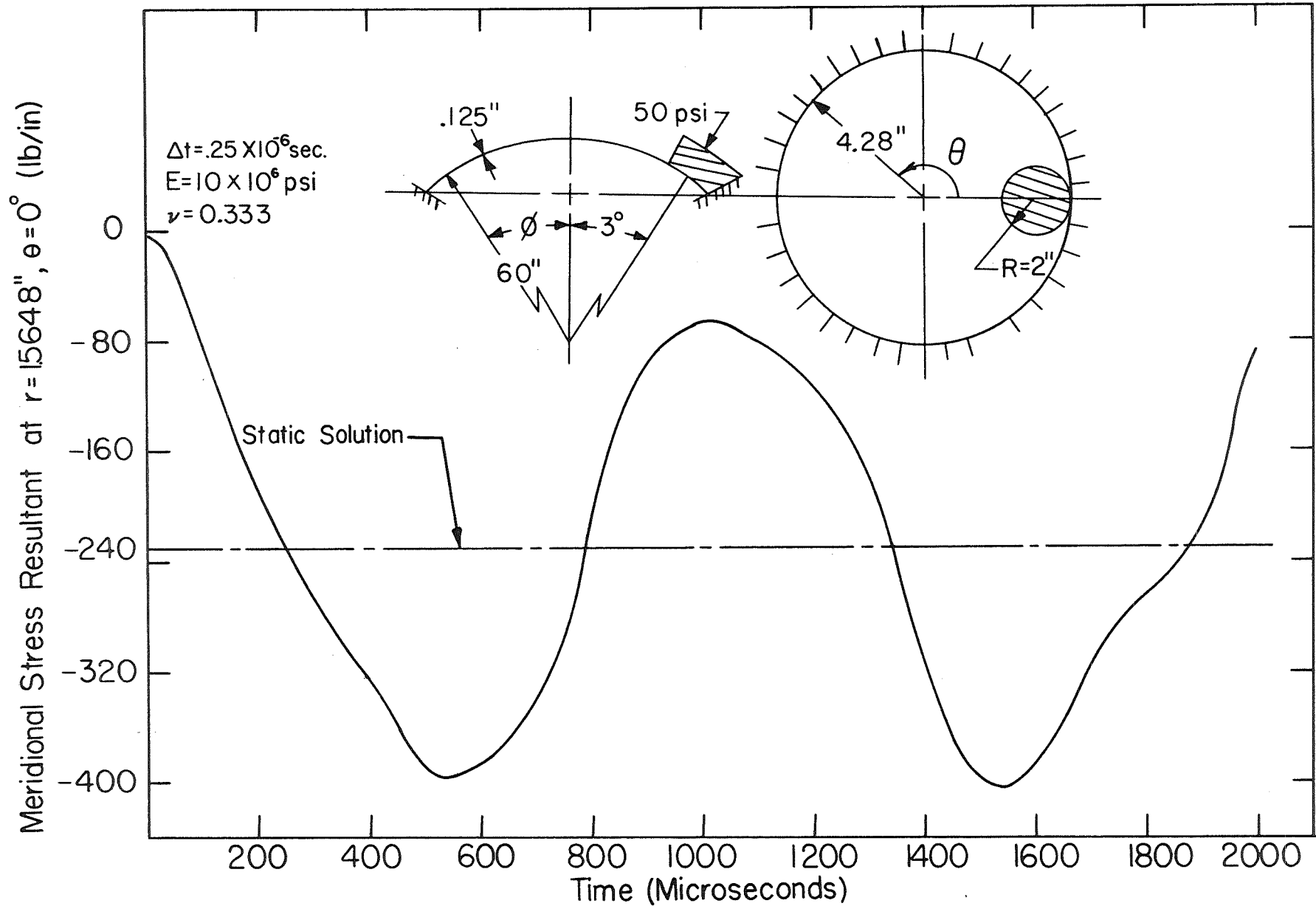


FIG. 24 MERIDIONAL STRESS RESULTANT FOR SPHERICAL CAP
UNDER LOCALIZED LOADING

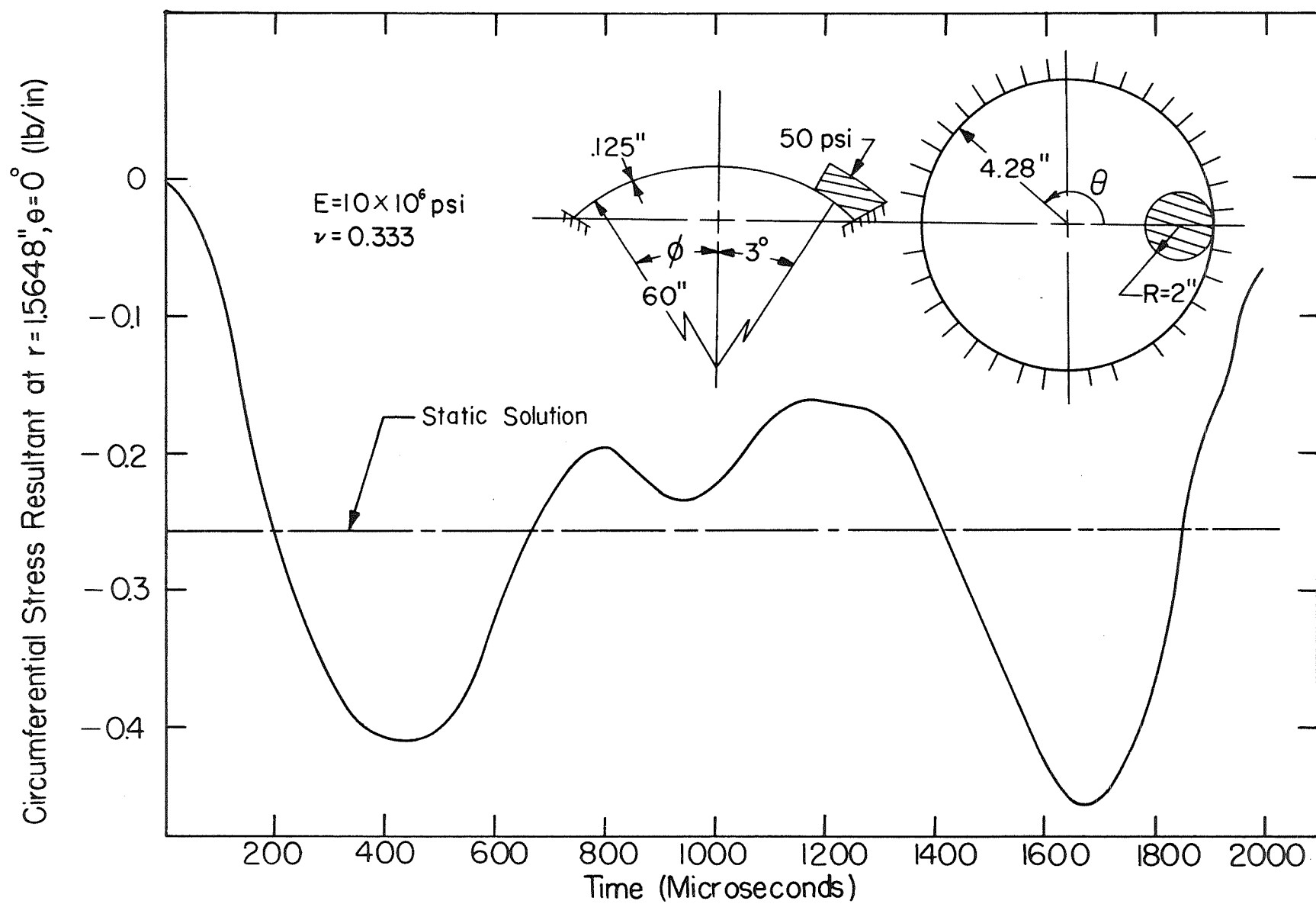


FIG. 25 CIRCUMFERENTIAL STRESS RESULTANT FOR SPHERICAL CAP UNDER LOCALIZED LOADING

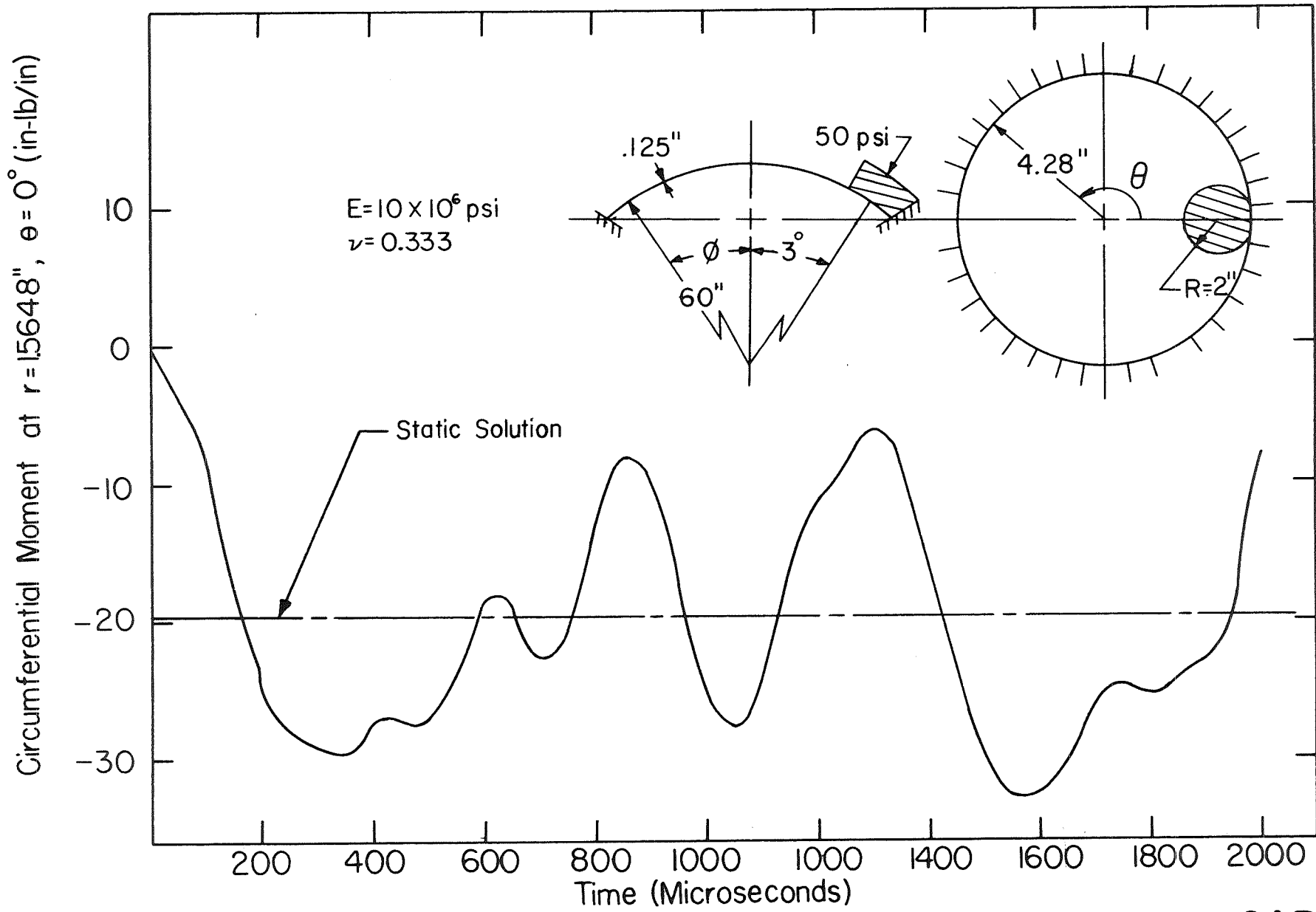


FIG. 26 CIRCUMFERENTIAL MOMENT FOR SPHERICAL CAP
UNDER LOCALIZED LOADING

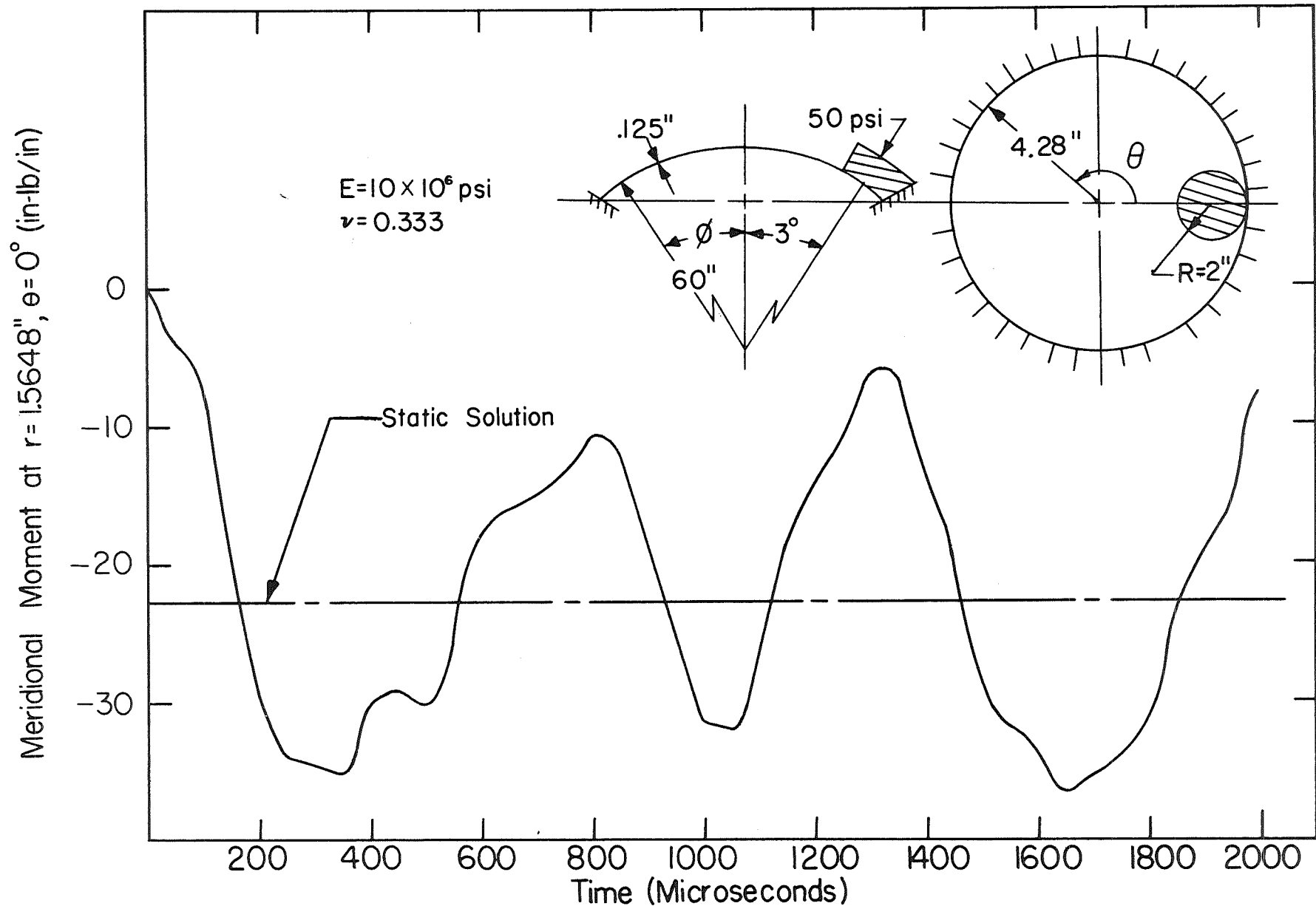


FIG. 27 MERIDIONAL MOMENT FOR SPHERICAL CAP UNDER
LOCALIZED LOADING

APPENDIX A

M A S S M A T R I X

Zero Harmonic

$$\bar{M}_{11} = 2\rho\pi t \int r ds$$

$$\bar{M}_{12} = 2\rho\pi t \int rs ds$$

$$\bar{M}_{13} = 2\rho\pi t \int rs^2 ds$$

$$\bar{M}_{14} = 2\rho\pi t \int rs^3 ds$$

$$\bar{M}_{15} = \bar{M}_{16} = \bar{M}_{17} = \bar{M}_{18} = 0$$

$$\bar{M}_{22} = 2\rho\pi t \int rs^2 ds + \frac{\rho\pi t^3}{6} \int r ds$$

$$\bar{M}_{23} = 2\rho\pi t \int rs^3 ds + \frac{\rho\pi t^3}{3} \int rs ds$$

$$\bar{M}_{24} = 2\rho\pi t \int rs^4 ds + \frac{\rho\pi t^3}{2} \int rs^2 ds$$

$$\bar{M}_{25} = \frac{\rho\pi t^3}{6} \int r\phi' ds$$

$$\bar{M}_{26} = \frac{\rho\pi t^3}{6} \int rs\phi' ds$$

$$\bar{M}_{27} = \bar{M}_{28} = 0$$

$$\bar{M}_{33} = 2\rho\pi t \int rs^4 ds + \frac{2\rho\pi t^3}{3} \int rs^2 ds$$

$$\bar{M}_{34} = 2\rho\pi t \int rs^5 ds + \rho\pi t^3 \int rs^3 ds$$

$$\bar{M}_{35} = \frac{\rho\pi t^3}{3} \int r\phi' s ds$$

$$\bar{M}_{36} = \frac{\rho\pi t^3}{3} \int r\phi' s^2 ds$$

$$\bar{M}_{37} = \bar{M}_{38} = 0$$

$$\bar{M}_{44} = 2\rho\pi t \int rs^6 ds + \frac{3\rho\pi t^3}{2} \int rs^4 ds$$

$$\bar{M}_{45} = \frac{\rho\pi t^3}{2} \int r\phi' s^2 ds$$

$$\bar{M}_{46} = \frac{\rho\pi t^3}{2} \int r\phi' s^3 ds$$

$$\bar{M}_{47} = \bar{M}_{48} = 0$$

$$\bar{M}_{55} = 2\rho\pi t \int r ds + \frac{\rho\pi t^3}{6} \int r \phi'^2 ds$$

$$\bar{M}_{56} = 2\rho\pi t \int rs ds + \frac{\rho\pi t^3}{6} \int r \phi'^2 s ds$$

$$\bar{M}_{57} = \bar{M}_{58} = 0$$

$$\bar{M}_{66} = 2\rho\pi t \int rs^2 ds + \frac{\rho\pi t^3}{6} \int r \phi'^2 s^2 ds$$

$$\bar{M}_{67} = \bar{M}_{68} = 0$$

$$\bar{M}_{77} = \bar{M}_{78} = \bar{M}_{88} = 0$$

i^{th} Harmonic

$$\bar{M}_{11} = \rho\pi t \int r ds + i^2 \frac{\rho\pi t^3}{12} \int \frac{ds}{r}$$

$$\bar{M}_{12} = \rho\pi t \int rs ds + i^2 \frac{\rho\pi t^3}{12} \int \frac{s ds}{r}$$

$$\bar{M}_{13} = \rho\pi t \int rs^2 ds + i^2 \frac{\rho\pi t^3}{12} \int \frac{s^2 ds}{r}$$

$$\bar{M}_{14} = \rho\pi t \int rs^3 ds + i^2 \frac{\rho\pi t^3}{12} \int s^3 ds$$

$$\bar{M}_{15} = \bar{M}_{16} = 0$$

$$\bar{M}_{17} = i \frac{\rho\pi t^3}{12} \int \frac{\cos\phi}{r} ds$$

$$\bar{M}_{18} = i \frac{\rho\pi t^3}{12} \int \frac{\cos\phi}{r} s ds$$

$$\bar{M}_{22} = \rho\pi t \int rs^2 ds + \frac{\rho\pi t^3}{12} \int r ds + i^2 \frac{\rho\pi t^3}{12} \int \frac{s^2 ds}{r}$$

$$\bar{M}_{23} = \rho\pi t \int rs^3 ds + \frac{\rho\pi t^3}{6} \int rs ds + i^2 \frac{\rho\pi t^3}{12} \int \frac{s^3 ds}{r}$$

$$\bar{M}_{24} = \rho\pi t \int rs^4 ds + \frac{\rho\pi t^3}{4} \int rs^2 ds + i^2 \frac{\rho\pi t^3}{12} \int \frac{s^4 ds}{r}$$

$$\bar{M}_{25} = \frac{\rho\pi t^3}{12} \int r \phi' ds$$

$$\bar{M}_{26} = \frac{\rho\pi t^3}{12} \int r \phi' s ds$$

$$\bar{M}_{27} = i \frac{\rho \pi t^3}{12} \int \frac{\cos \phi}{r} s ds$$

$$\bar{M}_{28} = i \frac{\rho \pi t^3}{12} \int \frac{\cos \phi}{r} s^2 ds$$

$$\bar{M}_{33} = \rho \pi t \int r s^4 ds + \frac{\rho \pi t^3}{3} \int r s^2 ds + i^2 \frac{\rho \pi t^3}{12} \int \frac{s^4 ds}{r}$$

$$\bar{M}_{34} = \rho \pi t \int r s^5 ds + \frac{\rho \pi t^3}{2} \int r s^3 ds + i^2 \frac{\rho \pi t^3}{12} \int \frac{s^5 ds}{r}$$

$$\bar{M}_{35} = \frac{\rho \pi t^3}{6} \int r \phi' s ds$$

$$\bar{M}_{36} = \frac{\rho \pi t^3}{6} \int r \phi' s^2 ds$$

$$\bar{M}_{37} = i \frac{\rho \pi t^3}{12} \int \frac{\cos \phi}{r} s^2 ds$$

$$\bar{M}_{38} = i \frac{\rho \pi t^3}{12} \int \frac{\cos \phi}{r} s^3 ds$$

$$\bar{M}_{44} = 3 \frac{\rho \pi t^3}{4} \int r s^4 ds + \rho \pi t \int r s^6 ds + i^2 \frac{\rho \pi t^3}{12} \int \frac{s^6 ds}{r}$$

$$\bar{M}_{45} = \frac{\rho \pi t^3}{4} \int r \phi' s^2 ds$$

$$\bar{M}_{46} = \frac{\rho \pi t^3}{4} \int r \phi' s^3 ds$$

$$\bar{M}_{47} = i \frac{\rho \pi t^3}{12} \int \frac{\cos \phi}{r} s^3 ds$$

$$\bar{M}_{48} = i \frac{\rho \pi t^3}{12} \int \frac{\cos \phi}{r} s^4 ds$$

$$\bar{M}_{55} = \rho \pi t \int r ds + \frac{\rho \pi t^3}{12} \int r \phi'^2 ds$$

$$\bar{M}_{56} = \rho \pi t \int r s ds + \frac{\rho \pi t^3}{12} \int r \phi'^2 s ds$$

$$\bar{M}_{57} = \bar{M}_{58} = 0$$

$$\bar{M}_{66} = \rho \pi t \int r s^2 ds + \frac{\rho \pi t^3}{12} \int r \phi'^2 s^2 ds$$

$$\bar{M}_{67} = \bar{M}_{68} = 0$$

$$\bar{M}_{77} = \rho \pi t \int r ds + \frac{\rho \pi t^3}{12} \int \frac{\cos^2 \phi}{r} ds$$

$$\bar{M}_{78} = \rho \pi t \int r s ds + \frac{\rho \pi t^3}{12} \int \frac{\cos^2 \phi}{r} s ds$$

$$\bar{M}_{88} = \rho \pi t \int r s^2 ds + \frac{\rho \pi t^3}{12} \int \frac{\cos^2 \phi}{r} s^2 ds$$

The mass matrix in structural coordinates is obtained from

$$[M^e] = [A]^T [\bar{M}] [A]$$

Appendix B. Linear Thermal Loads

Using the strain-displacement relations, the partial derivatives of U_L^t with respect to the coefficients, $\alpha_1, \alpha_2, \dots, \alpha_8$ can be obtained from Eq. 26 for harmonic $i > 0$:

$$\frac{\partial U_L^{ti}}{\partial \alpha_1^i} = -B_1 T^i \int \phi' r ds + B_2 T^i \int \cos\phi ds + B_4 T^i i^2 \int \frac{ds}{r}$$

$$\frac{\partial U_L^{ti}}{\partial \alpha_2^i} = -B_1 T^i \int \phi' s r ds + B_2 T^i \int s \cos\phi ds + B_4 T^i [i^2 \int \frac{s}{r} ds - \int s \sin\phi ds]$$

$$\frac{\partial U_L^{ti}}{\partial \alpha_3^i} = -B_1 T^i \int \phi' s^2 r ds + B_2 T^i \int s^2 \cos\phi ds - 2B_3 T^i \int r ds + B_4 T^i$$

$$[i^2 \int \frac{s^2}{r} ds - 2 \int s \sin\phi ds]$$

$$\frac{\partial U_L^{ti}}{\partial \alpha_4^i} = -B_1 T^i \int \phi' s^3 r ds + B_2 T^i \int s^3 \cos\phi ds - 6B_3 T^i \int s r ds + B_4 T^i$$

$$[i^2 \int \frac{s^3}{r} ds - 3 \int s^2 \sin\phi ds]$$

$$\frac{\partial U_L^{ti}}{\partial \alpha_5^i} = B_2 T^i \int \sin\phi ds - B_3 T^i \int \phi'' r ds - B_4 T^i \int \phi' \sin\phi r ds$$

$$\frac{\partial U_L^{ti}}{\partial \alpha_6^i} = B_1 T^i \int r ds + B_2 T^i \int s \sin\phi ds - B_3 T'^i \int (\phi''s + \phi') r ds \\ - B_4 T'^i \int s \phi' \sin\phi ds$$

$$\frac{\partial U_L^{ti}}{\partial \alpha_7^i} = B_2 T^i \int ds + B_4 T'^i \int \frac{\cos\phi}{r} ds$$

$$\frac{\partial U_L^{ti}}{\partial \alpha_8^i} = B_2 T^i \int s ds + B_4 T'^i \int \frac{s}{r} \cos\phi ds$$

where $B_1 = C_1 \pi (\alpha_s + v_{s\theta} \alpha_\theta)$

$$B_2 = C_2 \pi (\alpha_\theta + v_{\theta s} \alpha_s)$$

$$B_3 = D_1 \pi (\alpha_s + v_{s\theta} \alpha_\theta)$$

$$B_4 = D_2 \pi (\alpha_\theta + v_{\theta s} \alpha_s)$$

$$\phi' = \frac{d\phi}{ds}$$

$$\phi'' = \frac{d^2\phi}{ds^2}$$

For harmonic $i = 0$:

$$\frac{\partial U_L^{to}}{\partial \alpha_1^o} = 2[-B_1 T^o \int \phi' r ds + B_2 T^o \int \cos\phi ds]$$

$$\frac{\partial U_L^{to}}{\partial \alpha_2^o} = 2[-B_1 T^o \int \phi' s r ds + B_2 T^o \int s \cos\phi ds - B_4 T'^o \int s \sin\phi ds]$$

$$\begin{aligned} \frac{\partial U_L^{to}}{\partial \alpha_3^o} &= 2[-B_1 T^o \int \phi' s^2 r ds + B_2 T^o \int s^2 \cos\phi ds - 2B_3 T'^o \int r ds \\ &\quad - 2B_4 T'^o \int s \sin\phi ds] \end{aligned}$$

$$\begin{aligned} \frac{\partial U_L^{to}}{\partial \alpha_4^o} &= 2[-B_1 T^o \int \phi' s^3 r ds + B_2 T^o \int s^3 \cos\phi ds - 6B_3 T'^o \int s r ds \\ &\quad - 3B_4 T'^o \int s^2 \sin\phi ds] \end{aligned} \tag{B-2}$$

$$\frac{\partial U_L^{to}}{\partial \alpha_5^o} = 2[B_2 T^o \int \sin\phi ds - B_3 T'^o \int \phi'' r ds - B_4 T'^o \int \phi' \sin\phi r ds]$$

$$\begin{aligned} \frac{\partial U_L^{to}}{\partial \alpha_6^o} &= 2[B_1 T^o \int r ds + B_2 T^o \int s \sin\phi ds - B_3 T'^o \int (\phi'' s + \phi') r ds \\ &\quad - B_4 T'^o \int s \phi' \sin\phi ds] \end{aligned}$$

$$\frac{\partial U_L^{t_0}}{\partial \alpha_7^o} = 0$$

$$\frac{\partial U_L^{t_0}}{\partial \alpha_8^o} = 0$$